4. Incompressible Potential Flow Using Panel Methods

4.1 An Introduction

The incompressible potential flow model provides reliable flowfield predictions over a wide range of conditions. For the potential flow assumption to be valid for aerodynamics calculations the primary requirement is that viscous effects are small in the flowfield, and that the flowfield must be subsonic everywhere. Locally supersonic velocities can occur at surprisingly low freestream Mach numbers. For high-lift airfoils the peak velocities around the leading edge can become supersonic at freestream Mach numbers of 0.20 ~ 0.25. If the local flow is at such a low speed everywhere that it can be assumed incompressible (M .4, say), Laplace's Equation is essentially an exact representation of the inviscid flow. For higher subsonic Mach numbers with small disturbances to the freestream flow, the Prandtl-Glauert (P-G) Equation can be used. The P-G Equation can be converted to Laplace's Equation by a simple transformation.[1] This provides the basis for estimating the initial effects of compressibility on the flowfield, i.e., "linearized" subsonic flow. In both cases, the flowfield can be found by the solution of a single linear partial differential equation. Not only is the mathematical problem much simpler than any of the other equations that can be used to model the flowfield, but since the problem is linear, a large body of mathematical theory is available.

The Prandtl-Glauert Equation can also be used to describe supersonic flows. In that case the mathematical type of the equation is hyperbolic, and will be mentioned briefly in Chapter 12. Recall the important distinction between the two cases:

> subsonic flow: elliptic PDE, each point influences every other point,
>
> supersonic flow: hyperbolic PDE, discontinuities exist, "zone of influence" solution dependency.

In this chapter we consider incompressible flow only. One of the key features of Laplace's Equation is the property that allows the equation governing the flowfield to be converted from a 3D problem throughout the field to a 2D problem for finding the potential on the surface. The solution is then found using this property by distributing "singularities" of unknown strength over discretized portions of the surface: *panels*. Hence the flowfield solution is found by representing

the surface by a number of panels, and solving a linear set of algebraic equations to determine the unknown strengths of the singularities.[*] The flexibility and relative economy of the panel methods is so important in practice that the methods continue to be widely used despite the availability of more exact methods (which generally aren't yet capable of treating the range of geometries that the panel method codes can handle). An entry into the panel method literature is available through two recent reviews by Hess,[23] the survey by Erickson,[4] and the book by Katz and Plotkin.[5]

The general derivation of the integral equation for the potential solution of Laplace's equation is given in Section 4.3. Complete details are presented for one specific approach to solving the integral equation in Section 4.4. For clarity and simplicity of the algebra, the analysis will use the two-dimensional case to illustrate the methods following the analysis given by Moran.[6] This results in two ironic aspects of the presentation:

- The algebraic forms of the singularities are different between 2D and 3D, due to 3D relief. You can't use the actual formulas we derive in Section 4.4 for 3D problems.
- The power of panel methods arises in three-dimensional applications. Two-dimensional work in computational aerodynamics is usually done in industry using more exact mappings,[**] not panels.

After the general derivation, a panel method is used to examine the aerodynamics of airfoils. Finally, an example and some distinctive aspects of the 3D problem are presented.

4.2 Some Potential Theory

Potential theory is an extremely well developed (old) and elegant mathematical theory, devoted to the solution of Laplace's Equation:

$$\nabla^2 \phi = 0. \tag{4.1}$$

There are several ways to view the solution of this equation. The one most familiar to aerodynamicists is the notion of "singularities". These are algebraic functions which satisfy Laplace's equation, and can be combined to construct flowfields. Since the equation is linear, superposition of solutions can be used. The most familiar singularities are the point source, doublet and vortex. In classical examples the singularities are located inside the body. Unfortunately, an arbitrary body shape cannot be created using singularities placed inside the body. A more sophisticated approach has to be used to determine the potential flow over arbitrary shapes. Mathematicians have developed this theory. We will draw on a few selected results to help understand the development of panel methods. Initially, we are interested in the specification of the boundary conditions. Consider the situation illustrated Fig. 4-1.

---

[*] The singularities are distributed across the panel. They are not specified at a point. However, the boundary conditions usually are satisfied at a specific location.
[**] These will be mentioned in more detail in Chapter 9.
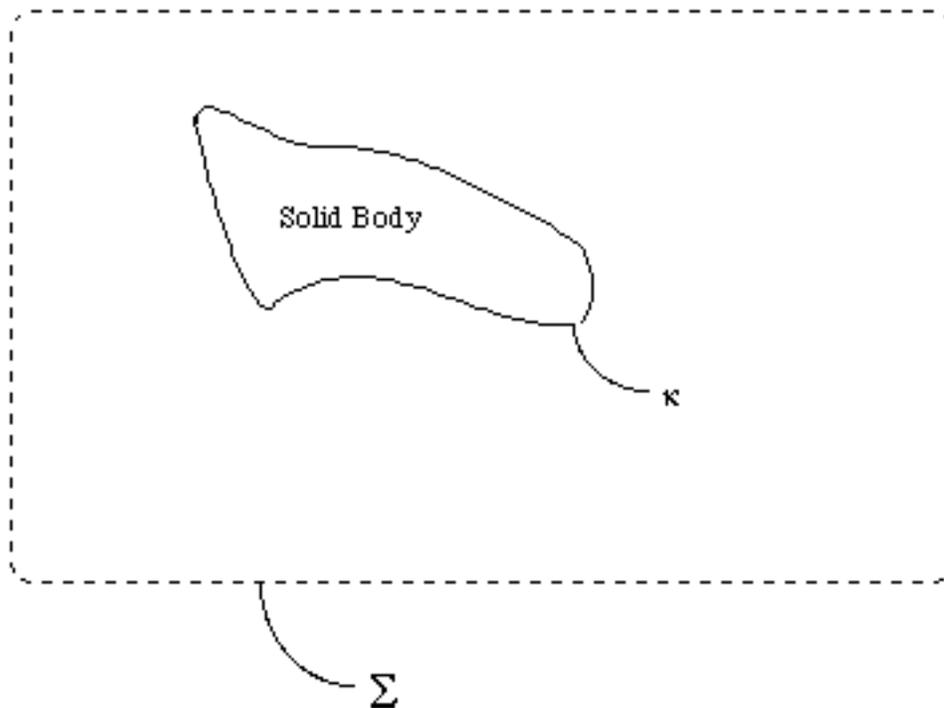
Figure 4-1. Boundaries for flowfield analysis.

The flow pattern is uniquely determined by giving either:

$$\phi \quad \text{on} \quad + \quad \{\text{Dirichlet Problem: Design}\} \tag{4-2}$$

or

$$\partial\phi/\partial n \quad \text{on} \quad + \quad \{\text{Neuman Problem: Analysis}\}. \tag{4-3}$$

Potential flow theory states that you cannot specify both arbitrarily, but can have a mixed boundary condition, $a\phi + b \, \partial\phi/\partial n$ on $+$. The Neumann Problem is identified as "analysis" above because it naturally corresponds to the problem where the flow through the surface is specified (usually zero). The Dirichlet Problem is identified as "design" because it tends to correspond to the aerodynamic case where a surface pressure distribution is specified and the body shape corresponding to the pressure distribution is sought. Because of the wide range of problem formulations available in linear theory, some analysis procedures appear to be Dirichlet problems, but Eq. (4-3) must still be used.

Some other key properties of potential flow theory:

- If either ϕ or $\partial\phi/\partial n$ is zero everywhere on $+$ then $\phi = 0$ at all interior points.

- ϕ cannot have a maximum or minimum at any interior point. Its maximum value can only occur on the surface boundary, and therefore the minimum pressure (and maximum velocity) occurs on the surface.

4.3 Derivation of the Integral Equation for the Potential

We need to obtain the equation for the potential in a form suitable for use in panel method calculations. This section follows the presentation given by Karamcheti[7] on pages 344-348 and Katz and Plotkin[5] on pages 52-58. An equivalent analysis is given by Moran[6] in his Section 8.1. The objective is to obtain an expression for the potential anywhere in the flowfield in terms of values on the surface bounding the flowfield. Starting with the Gauss Divergence Theorem, which relates a volume integral and a surface integral,

$$\int_R \operatorname{div} \mathbf{A}\, dV = \oint_S \mathbf{A} \cdot \mathbf{n}\, dS \tag{4-4}$$

we follow the classical derivation and consider the interior problem as shown in Fig. 4-2.
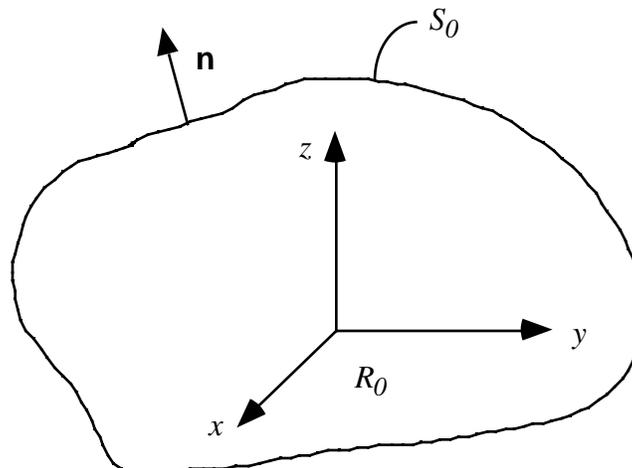
Figure 4-2. Nomenclature for integral equation derivation.

To start the derivation introduce the vector function of two scalars:

$$\mathbf{A} = \operatorname{grad} \quad - \quad \operatorname{grad} \quad . \tag{4-5}$$

Substitute this function into the Gauss Divergence Theorem, Eq. (4-4), to obtain:

$$\int_R \operatorname{div}\left(\operatorname{grad} \quad - \quad \operatorname{grad} \quad \right) dV = \oint_S \left(\operatorname{grad} \quad - \quad \operatorname{grad} \quad \right) \mathbf{n}\, dS. \tag{4-6}$$

Now use the vector identity: $\quad \mathbf{F} = \quad \mathbf{F} + \mathbf{F} \quad$ to simplify the left hand side of Eq. (4-6). Recalling that $\quad \mathbf{A} = \operatorname{div} \mathbf{A}$, write the integrand of the LHS of Eq. (4-6) as:

$$\operatorname{div}\left(\operatorname{grad} \quad - \quad \operatorname{grad} \quad \right) = \quad \left(\quad \right) - \quad \left(\quad \right)$$
$$= \quad + \quad - \quad - \tag{4-7}$$
$$= \quad ^2 \quad - \quad ^2$$

Substituting the result of Eq. (4-7) for the integrand in the LHS of Eq. (4-6), we obtain:

$$\int_R \left(\phi \nabla^2 \psi - \psi \nabla^2 \phi \right) dV = \oint_S \left(\phi \, grad \, \psi - \psi \, grad \, \phi \right) \mathbf{n} \, dS, \tag{4-8}$$

or equivalently (recalling that $grad \, \phi \cdot \mathbf{n} = \partial \phi / \partial n$),

$$\int_R \left(\phi \nabla^2 \psi - \psi \nabla^2 \phi \right) dV = \oint_S \left(\phi \frac{\partial \psi}{\partial n} - \psi \frac{\partial \phi}{\partial n} \right) dS. \tag{4-9}$$

Either statement is known as Green's theorem of the second form.

Now, define $\phi = 1/r$ and $\psi = \Phi$, where Φ is a harmonic function (a function that satisfies Laplace's equation). The $1/r$ term is a source singularity in three dimensions. This makes our analysis three-dimensional. In two dimensions the form of the source singularity is $\ln r$, and a two-dimensional analysis starts by defining $\phi = \ln r$. Now rewrite Eq. (4-8) using the definitions of ϕ and ψ given at the first of this paragraph and switch sides,

$$\oint_{S_0} \left(\frac{1}{r} \frac{\partial \Phi}{\partial n} - \Phi \frac{\partial}{\partial n} \frac{1}{r} \right) \mathbf{n} \, dS = \int_{R_0} \left(\frac{1}{r} \nabla^2 \Phi - \Phi \nabla^2 \frac{1}{r} \right) dV. \tag{4-10}$$

R_0 is the region enclosed by the surface S_0. Recognize that on the right hand side the first term, $\nabla^2 \Phi$, is equal to zero by definition so that Eq. (4-10) becomes

$$\oint_{S_0} \left(\frac{1}{r} \frac{\partial \Phi}{\partial n} - \Phi \frac{\partial}{\partial n} \frac{1}{r} \right) \mathbf{n} \, dS = - \int_{R_0} \Phi \nabla^2 \frac{1}{r} \, dV. \tag{4-11}$$

If a point P is external to S_0, then $\nabla^2 \frac{1}{r} = 0$ everywhere since $1/r$ is a source, and thus satisfies Laplace's Equation. This leaves the RHS of Eq. (4-11) equal to zero, with the following result:

$$\oint_{S_0} \left(\frac{1}{r} \frac{\partial \Phi}{\partial n} - \Phi \frac{\partial}{\partial n} \frac{1}{r} \right) \mathbf{n} \, dS = 0. \tag{4-12}$$

However, we *have* included the origin in our region S_0 as defined above. If P is inside S_0, then $\nabla^2 \frac{1}{r} \to \infty$ at $r = 0$. Therefore, we exclude this point by defining a new region which excludes the origin by drawing a sphere of radius ε around $r = 0$, and applying Eq. (4-12) to the region between ε and S_0:

$$\underbrace{\oint_{S_0}\left[\frac{1}{r}\quad-\quad\frac{1}{r}\right]\mathbf{n}\,dS}_{\text{arbitrary region}}-\underbrace{\oint\left[\frac{1}{r}\frac{}{r}+\frac{}{r^2}\right]dS}_{\text{sphere}}=0 \qquad (4\text{-}13)$$

or:

$$\oint\left[\frac{1}{r}\frac{}{r}+\frac{}{r^2}\right]dS=\oint_{S_0}\left[\frac{1}{r}\quad-\quad\frac{1}{r}\right]\mathbf{n}\,dS. \qquad (4\text{-}14)$$

Consider the first integral on the left hand side of Eq. (4-14). Let   0, where (as   0) we take   constant ($/\ r=0$), assuming that   is well-behaved and using the mean value theorem. Then we need to evaluate

$$\oint\frac{dS}{r^2}$$

over the surface of the sphere where $= r$. Recall that for a sphere[*] the elemental area is

$$dS = r^2\sin\ d\ d \qquad (4\text{-}15)$$

where we define the angles in Fig. 4-3. Do not confuse the classical notation for the spherical coordinate angles with the potential function. The spherical coordinate   will disappear as soon as we evaluate the integral.
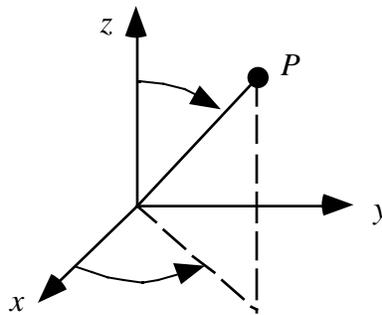
Figure 4-3. Spherical coordinate system nomenclature.

Substituting for dS in the integral above, we get:

$$\oint\sin\ d\ d\ .$$

Integrating from $= 0$ to   , and   from 0 to 2 , we get:

[*] See Hildebrand, F.B., *Advanced Calculus for Applications*, 2nd Ed., Prentice-Hall, Englewood Cliffs, 1976 for an excellent review of spherical coordinates and vector analysis.

$$\int_{\phi=0}^{2\pi}\int_{\theta=0}^{\pi}\sin\theta\, d\theta\, d\phi = 4\pi \, .$$ (4-16)

The final result for the first integral in Eq. (4-14) is:

$$\oint \left[\frac{1}{r}\frac{\partial}{\partial r} + \frac{1}{r^2} \right] dS = 4\pi \, .$$ (4-17)

Replacing this integral by its value from Eq. (4-17) in Eq. (4-14), we can write the expression for the potential at any point P as (where the origin can be placed anywhere inside S_0):

$$\Phi(p) = \frac{1}{4\pi}\oint_{s0} \left[\frac{1}{r}\nabla\Phi - \Phi\nabla\frac{1}{r} \right]\cdot\mathbf{n}\,dS$$ (4-18)

and the value of Φ at any point P is now known as a function of Φ and $\partial\Phi/\partial n$ on the boundary.

We used the interior region to allow the origin to be written at point P. This equation can be extended to the solution for Φ for the region exterior to R_0. Apply the results to the region between the surface S_B of the body and an arbitrary surface Σ enclosing S_B and then let Σ go to infinity. The integrals over Σ go to Φ_∞ as Σ goes to infinity. Thus potential flow theory is used to obtain the important result that the potential at any point P' in the flowfield outside the body can be expressed as:

$$\Phi(p') = \Phi_\infty -\frac{1}{4\pi}\oint_{S_B} \left[\frac{1}{r}\nabla\Phi - \Phi\nabla\frac{1}{r} \right]\cdot\mathbf{n}\,dS.$$ (4-19)

Here the unit normal $\mathbf{n}$ is now considered to be pointing outward and the area can include not only solid surfaces but also wakes. Equation 4-19 can also be written using the dot product of the normal and the gradient as:

$$\Phi(p') = \Phi_\infty -\frac{1}{4\pi}\oint_{S_B} \left[\frac{1}{r}\frac{\partial\Phi}{\partial n} - \Phi\frac{\partial}{\partial n}\frac{1}{r} \right] dS.$$ (4-20)

The $1/r$ in Eq. (4-19) can be interpreted as a source of strength $\partial\Phi/\partial n$, and the $\nabla(1/r)$ term in Eq. (4-19) as a doublet of strength Φ. Both of these functions play the role of Green's functions in the mathematical theory. Therefore, we can find the potential as a function of a distribution of sources and doublets over the surface. *The integral in Eq. (4-20) is normally broken up into body and wake pieces*. The wake is generally considered to be infinitely thin. Therefore, only doublets are used to represent the wakes.

Now consider the potential to be given by the superposition of two different known functions, the first and second terms in the integral, Eq. (4-20). These can be taken to be the distribution of the source and doublet strengths, and μ, respectively. Thus Eq (4-20) can be written in the form usually seen in the literature,

$$\phi(p) = -\frac{1}{4\pi} \oint_{S_B} \left[\sigma \frac{1}{r} - \mu \frac{\partial}{\partial n} \frac{1}{r} \right] dS. \qquad (4-21)$$

The problem is to find the values of the unknown source and doublet strengths and μ for a specific geometry and given freestream, .

What just happened? We replaced the requirement to find the solution over the entire flowfield (a 3D problem) with the problem of finding the solution for the singularity distribution over a surface (a 2D problem). In addition, we now have an integral equation to solve for the unknown surface singularity distributions instead of a partial differential equation. The problem is linear, allowing us to use superposition to construct solutions. We also have the freedom to pick whether to represent the solution as a distribution of sources or doublets distributed over the surface. In practice it's been found best to use a combination of sources and doublets. The theory can be extended to include other singularities.

At one time the change from a 3D to a 2D problem was considered significant. However, the total information content is the same computationally. This shows up as a dense "2D" matrix vs. a sparse "3D" matrix. As methods for sparse matrix solutions evolved, computationally the problems became nearly equivalent. The advantage in using the panel methods arises because there is no need to define a grid throughout the flowfield.

This is the theory that justifies panel methods, i.e., that we can represent the surface by panels with distributions of singularities placed on them. Special precautions must be taken when applying the theory described here. Care should be used to ensure that the region S_B is in fact completely closed. In addition, care must be taken to ensure that the outward normal is properly defined.

Furthermore, in general, the interior problem cannot be ignored. Surface distributions of sources and doublets affect the interior region as well as exterior. In some methods the interior problem is implicitly satisfied. In other methods the interior problem requires explicit attention. The need to consider this subtlety arose when advanced panel methods were developed. The problem is not well posed unless the interior problem is considered, and numerical solutions failed when this aspect of the problem was not addressed. References 4 and 5 provide further discussion.

When the exterior and interior problems are formulated properly the boundary value problem is properly posed. Additional discussions are available in the books by Ashley and Landahl[8] and Curle and Davis.[9]

We implement the ideas give above by:

a) approximating the surface by a series of line segments (2D) or panels (3D)
b) placing distributions of sources and vortices or doublets on each panel.

There are many ways to tackle the problem (and many competing codes). Possible differences in approaches to the implementation include the use of:

- various singularities
- various distributions of the singularity strength over each panel
- panel geometry (panels don't have to be flat).

Recall that superposition allows us to construct the solution by adding separate contributions [Watch out! You have to get all of them. Sometimes this can be a problem]. Thus we write the potential as the sum of several contributions. Figure 4-4 provides an example of a panel representation of an airplane. The wakes are not shown, and a more precise illustration of a panel method representation is given in Section 4.8.
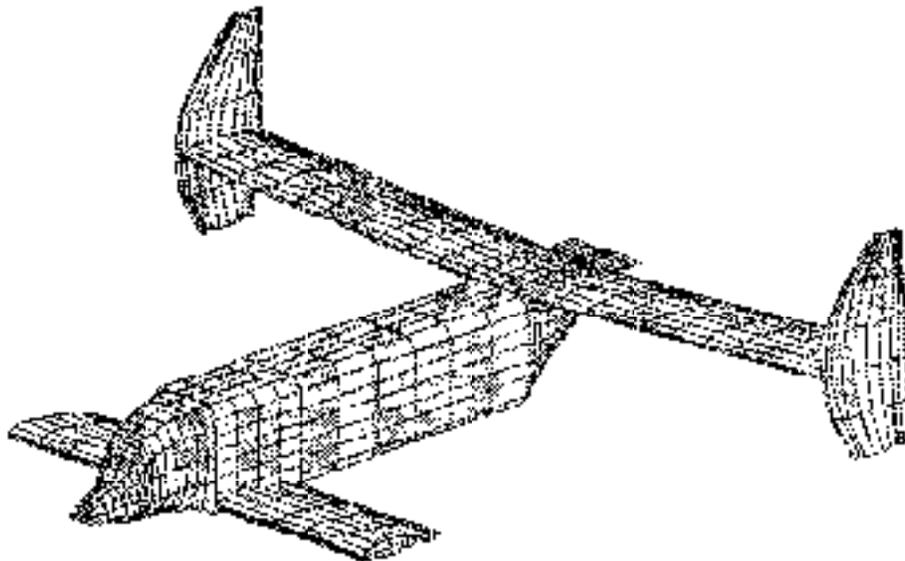
Figure 4-4. Panel model representation of an airplane.
(Joe Mazza, M.S. Thesis, Virginia Tech, 1993).

An example of the implementation of a panel method is carried out in Section 4.4 in two dimensions. To do this, we write down the two-dimensional version of Eq. (4-21). In addition, we use a vortex singularity in place of the doublet singularity (Ref. 4 and 5 provide details on this change). The resulting expression for the potential is:

$$
\phi = \underbrace{\phi_\infty}_{\substack{\text{uniform onset flow} \\ = V_\infty x \cos\alpha + V_\infty y \sin\alpha}} + \int_S \left[\underbrace{\frac{q(s)}{2\pi} \ln r}_{\substack{q \text{ is the 2D} \\ \text{source strength}}} - \underbrace{\frac{\gamma(s)}{2\pi}\theta}_{\substack{\text{this is a vortex singularity} \\ \text{of strength } \gamma(s)}} \right] ds \qquad (4\text{-}22)
$$

and $\theta = \tan^{-1}(y/x)$. Although the equation above shows contributions from various components of the flowfield, the relation is still exact. No small disturbance assumption has been made.

4.4 The Classic Hess and Smith Method

A.M.O. Smith at Douglas Aircraft directed an incredibly productive aerodynamics development group in the late '50s through the early '70s. In this section we describe the implementation of the theory given above that originated in his group.[*] Our derivation follows Moran's description[6] of the Hess and Smith method quite closely. The approach is to *i*) break up the surface into straight line segments, *ii*) assume the source strength is constant over each line segment (panel) but has a different value for each panel, and *iii*) the vortex strength is constant and equal over each panel.

Roughly, think of the constant vortices as adding up to the circulation to satisfy the Kutta condition. The sources are required to satisfy flow tangency on the surface (thickness).

Figure 4-5 illustrates the representation of a smooth surface by a series of line segments. The numbering system starts at the lower surface trailing edge and proceeds forward, around the leading edge and aft to the upper surface trailing edge. *N*+1 points define *N* panels.
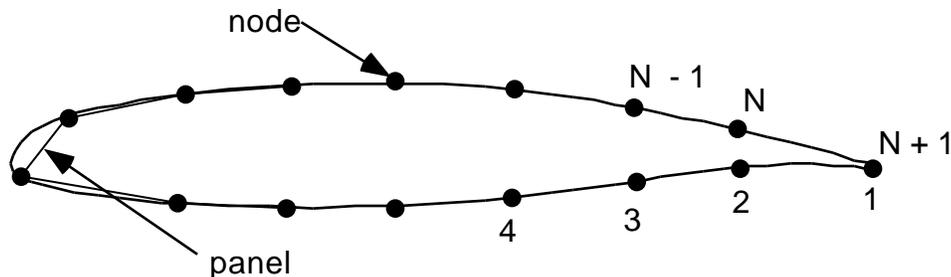
Figure 4-5. Representation of a smooth airfoil with straight line segments.

The potential relation given above in Eq. (4-22) can then be evaluated by breaking the integral up into segments along each panel:

$$
\phi = V_\infty \left(x \cos\alpha + y \sin\alpha \right) + \sum_{j=1}^{N} \int_{\text{panel } j} \left[\frac{q(s)}{2\pi} \ln r - \frac{\gamma}{2\pi}\theta \right] dS \qquad (4\text{-}23)
$$

---

with $q(s)$ taken to be constant on each panel, allowing us to write $q(s) = q_i$, $i = 1, \ldots N$. Here we need to find N values of q_i and one value of .

a) basic nomenclature   b) unit vector orientation
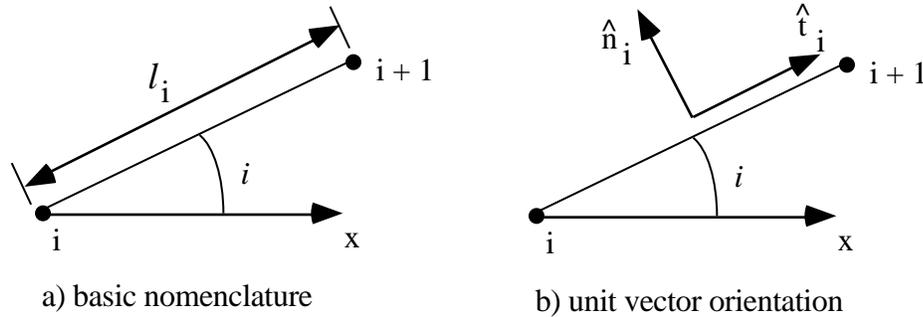
Figure 4-6. Nomenclature for local coordinate systems.

Use Figure 4-6 to define the nomenclature on each panel. Let the ith panel be the one between the ith and $i+1^{th}$ nodes, and let the ith panel's inclination to the x axis be . Under these assumptions the sin and cos of are given by:

$$\sin_i = \frac{y_{i+1} - y_i}{l_i}, \qquad \cos_i = \frac{x_{i+1} - x_i}{l_i} \tag{4-24}$$

and the normal and tangential unit vectors are:

$$\begin{aligned} \mathbf{n}_i &= -\sin_i \mathbf{i} + \cos_i \mathbf{j} \\ \mathbf{t}_i &= \cos_i \mathbf{i} + \sin_i \mathbf{j} \end{aligned} \tag{4-25}$$

We will find the unknowns by satisfying the flow tangency condition on each panel at one specific control point (also known as a collocation point) and requiring the solution to satisfy the Kutta condition. The control point will be picked to be at the mid-point of each panel, as shown in Fig. 4-7.
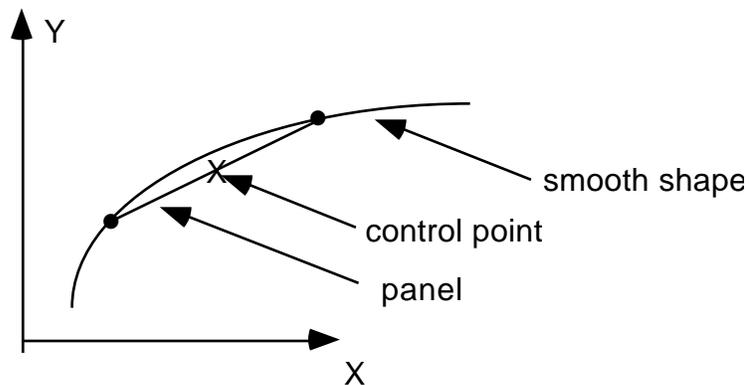
Figure 4-7. Local panel nomenclature.

Thus the coordinates of the midpoint of the control point are given by:

$$\bar{x}_i = \frac{x_i + x_{i+1}}{2}, \qquad \bar{y}_i = \frac{y_i + y_{i+1}}{2} \tag{4-26}$$

and the velocity components at the control point $\bar{x}_i$, $\bar{y}_i$ are $u_i = u(\bar{x}_i, \bar{y}_i)$, $v_i = v(\bar{x}_i, \bar{y}_i)$.

The flow tangency boundary condition is given by $\mathbf{V} \cdot \mathbf{n} = 0$, and is written using the relations given here as:

$$\left(u_i\mathbf{i} + v_i\mathbf{j}\right) \cdot \left(-\sin\,_i\mathbf{i} + \cos\,_i\mathbf{j}\right) = 0$$

or

$$-u_i \sin\,_i + v_i \cos\,_i = 0, \quad \text{for each } i, \ i = 1, \dots, N. \tag{4-27}$$

The remaining relation is found from the Kutta condition. This condition states that the flow must leave the trailing edge smoothly. Many different numerical approaches have been adopted to satisfy this condition. In practice this implies that at the trailing edge the pressures on the upper and lower surface are equal. Here we satisfy the Kutta condition approximately by equating velocity components tangential to the panels adjacent to the trailing edge on the upper and lower surface. Because of the importance of the Kutta condition in determining the flow, the solution is extremely sensitive to the flow details at the trailing edge. When we make the assumption that the velocities are equal on the top and bottom panels at the trailing edge we need to understand that we must make sure that the last panels on the top and bottom are small and of equal length. Otherwise we have an inconsistent approximation. Accuracy will deteriorate rapidly if the panels are not the same length. We will develop the numerical formula using the nomenclature for the trailing edge shown in Fig. 4-8.
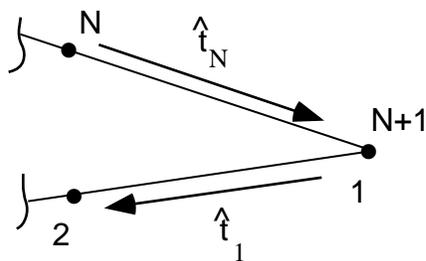
Figure 4-8. Trailing edge panel nomenclature.

Equating the magnitude of the tangential velocities on the upper and lower surface:

$$u_{t_1} = u_{t_N}. \tag{4-28}$$

and taking the difference in direction of the tangential unit vectors into account this is written as

$$\mathbf{V} \cdot \mathbf{t}\big|_1 = -\mathbf{V} \cdot \mathbf{t}\big|_N. \tag{4-29}$$

Carrying out the operation we get the relation:

$$\left(u_1\mathbf{i} + v_1\mathbf{j}\right)\left(\cos_1\mathbf{i} + \sin_1\mathbf{j}\right) = -\left(u_N\mathbf{i} + v_N\mathbf{j}\right)\left(\cos_N\mathbf{i} + \sin_N\mathbf{j}\right)$$

which is expanded to obtain the final relation:

$$u_1\cos_1 + v_1\sin_1 = -u_N\cos_N + v_N\sin_N \tag{4-30}$$

The expression for the potential in terms of the singularities on each panel and the boundary conditions derived above for the flow tangency and Kutta condition are used to construct a system of linear algebraic equations for the strengths of the sources and the vortex. The steps required are summarized below. Then we will carry out the details of the algebra required in each step.

Steps to determine the solution:

1. Write down the velocities, u_i, v_i, in terms of contributions from all the singularities. This includes q_i, from each panel and the influence coefficients which are a function of the geometry only.

2. Find the algebraic equations defining the "influence" coefficients.

To generate the system of algebraic equations:

3. Write down flow tangency conditions in terms of the velocities (N eqn's., $N+1$ unknowns).

4. Write down the Kutta condition equation to get the $N+1$ equation.

5. Solve the resulting linear algebraic system of equations for the q_i, .

6. Given q_i, , write down the equations for u_{ti}, the tangential velocity at each panel control point.

7. Determine the pressure distribution from Bernoulli's equation using the tangential velocity on each panel.

We now carry out each step in detail. The algebra gets tedious, but there's no problem in carrying it out. As we carry out the analysis for two dimensions, consider the additional algebra required for the general three dimensional case.

Step 1. Velocities

The velocity components at any point *i* are given by contributions from the velocities induced by the source and vortex distributions over each panel. The mathematical statement is:

$$u_i = V_\infty \cos\alpha + \sum_{j=1}^{N} q_j u_{s_{ij}} + \sum_{j=1}^{N} \gamma\, u_{v_{ij}}$$

$$v_i = V_\infty \sin\alpha + \sum_{j=1}^{N} q_j v_{s_{ij}} + \sum_{j=1}^{N} \gamma\, v_{v_{ij}} \tag{4-31}$$

where q_i and γ are the singularity strengths, and the $u_{s_{ij}}$, $v_{s_{ij}}$, $u_{v_{ij}}$, and $v_{v_{ij}}$ are the influence coefficients. As an example, the influence coefficient $u_{s_{ij}}$ is the *x*-component of velocity at x_i due to a unit source distribution over the *j*th panel.

Step 2. Influence coefficients

To find $u_{s_{ij}}$, $v_{s_{ij}}$, $u_{v_{ij}}$, and $v_{v_{ij}}$ we need to work in a local panel coordinate system x^*, y^* which leads to a straightforward means of integrating source and vortex distributions along a straight line segment. This system will be locally aligned with each panel *j*, and is connected to the global coordinate system as illustrated in Fig. 4-9.
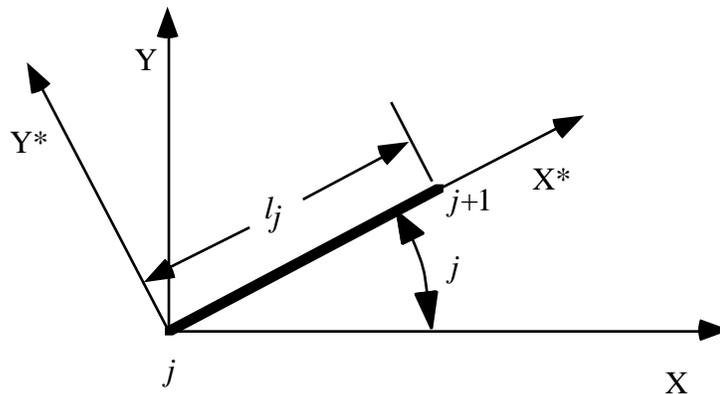
Figure 4-9. Local panel coordinate system and nomenclature.

The influence coefficients determined in the local coordinate system aligned with a particular panel are u^* and v^*, and are transformed back to the global coordinate system by:

$$u = u^* \cos\theta_j - v^* \sin\theta_j$$

$$v = u^* \sin\theta_j + v^* \cos\theta_j \tag{4-32}$$

We now need to find the velocities induced by the singularity distributions. We consider the source distributions first. The velocity field induced by a source in its natural cylindrical coordinate system is:

$$\mathbf{V} = \frac{Q}{2 \; r}\,\hat{\mathbf{e}}_{\mathbf{r}}. \tag{4-33}$$

Rewriting in Cartesian coordinates (and noting that the source described in Eq. (4-33) is located at the origin, $r = 0$) we have:

$$u(x,y) = \frac{Q}{2}\frac{x}{x^2 + y^2}, \qquad v(x,y) = \frac{Q}{2}\frac{y}{x^2 + y^2}. \tag{4-34}$$

In general, if we locate the sources along the x-axis at a point $x = t$, and integrate over a length l, the velocities induced by the source distributions are obtained from:

$$
\begin{aligned}
u_s &= \int_{t=0}^{t=l} \frac{q(t)}{2} \frac{x - t}{(x - t)^2 + y^2}\,dt \\[2mm]
v_s &= \int_{t=0}^{t=l} \frac{q(t)}{2} \frac{y}{(x - t)^2 + y^2}\,dt
\end{aligned}
\tag{4-35}
$$

To obtain the influence coefficients, write down this equation in the ( )* coordinate system, with $q(t) = 1$ (unit source strength):

$$
\begin{aligned}
u^*_{s_{ij}} &= \frac{1}{2}\int_0^{l_j} \frac{x^*_i - t}{(x^*_i - t)^2 + y^{*2}_i}\,dt \\[2mm]
v^*_{s_{ij}} &= \frac{1}{2}\int_0^{l_j} \frac{y^*_i}{(x^*_i - t)^2 + y^{*2}_i}\,dt
\end{aligned}
\tag{4-36}
$$

These integrals can be found (from tables) in closed form:

$$
\begin{aligned}
u^*_{s_{ij}} &= -\frac{1}{2}\ln\left[\left(x^*_i - t\right)^2 + y^{*2}_i\right]^{\frac{1}{2}}\Bigg|_{t=0}^{t=l_j} \\[3mm]
v^*_{s_{ij}} &= \frac{1}{2}\tan^{-1}\frac{y^*_i}{x^*_i - t}\Bigg|_{t=0}^{t=l_j}
\end{aligned}
\tag{4-37}
$$

To interpret these expressions examine Fig. 4-10. The notation adopted and illustrated in the sketch makes it easy to translate the results back to global coordinates.

2/24/98
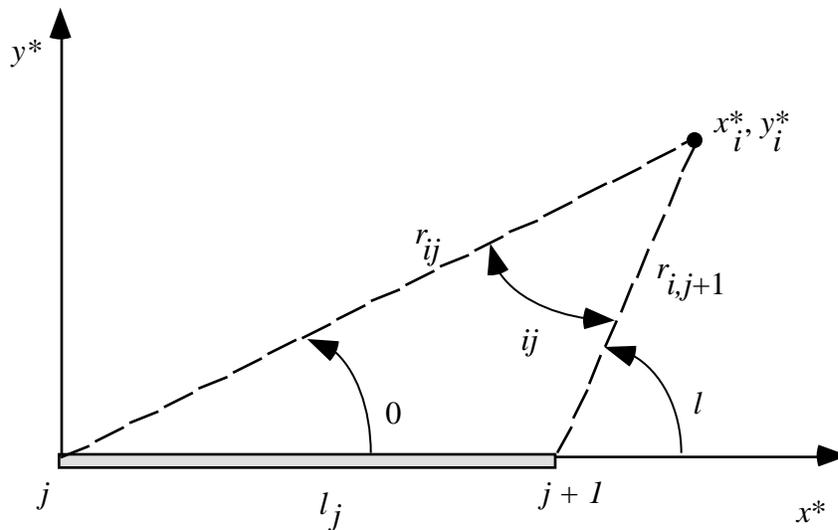
Figure 4-10. Relations between the point x*, y* and a panel.

Note that the formulas for the integrals given in Eq. (4-37) can be interpreted as a radius and an angle. Substituting the limits into the expressions and evaluating results in the final formulas for the influence coefficients due to the sources:

$$u_{s_{ij}}^* = -\frac{1}{2} \ln \frac{r_{i,j+1}}{r_{ij}}$$

$$v_{s_{ij}}^* = \frac{\nu_l - \nu_0}{2} = \frac{\nu_{ij}}{2}$$

(4-38)

Here r_{ij} is the distance from the jth node to the point i, which is taken to be the control point location of the ith panel. The angle ν_{ij} is the angle subtended at the middle of the ith panel by the jth panel.

The case of determining the influence coefficient for a panel's influence on itself requires some special consideration. Consider the influence of the panel source distribution on itself. The source induces normal velocities, and no tangential velocities, Thus, $u_{s_{ii}}^* = 0$ and $v_{s_{ii}}^*$ depends on the side from which you approach the panel control point. Approaching the panel control point from the outside leads to $\nu_{ii} = \pi$, while approaching from inside leads to $\nu_{ii} = -\pi$. Since we are working on the exterior problem,

$$\nu_{ii} = \pi ,$$

(4-39)

and to keep the correct sign on $\nu_{ij}, j \neq i$, use the FORTRAN subroutine ATAN2, which takes into account the correct quadrant of the angle.[*]

---

[*] Review a FORTRAN manual to understand how ATAN2 is used.

Now consider the influence coefficients due to vortices. There is a simple connection between source and vortex flows that allows us to use the previous results obtained for the source distribution directly in the vortex singularity distribution analysis.

The velocity due to a point vortex is usually given as:

$$V = -\frac{}{2}\frac{}{r}\mathbf{e} \ . \tag{4-40}$$

Compared to the source flow, the u, v components simply trade places (with consideration of the direction of the flow to define the proper signs). In Cartesian coordinates the velocity due to a point vortex is:

$$u(x,y) = +\frac{}{2}\frac{y}{x^2 + y^2}, \qquad v(x,y) = -\frac{}{2}\frac{x}{x^2 + y^2} \ . \tag{4-41}$$

where the origin (the location of the vortex) is $x = y = 0$.

Using the same analysis used for source singularities for vortex singularities the equivalent vortex distribution results can be obtained. Summing over the panel with a vortex strength of unity we get the formulas for the influence coefficients due to the vortex distribution:

$$
\begin{aligned}
u^*_{v_{ij}} &= +\frac{1}{2} \int_0^{l_j} \frac{y^*_i}{(x^*_i - t)^2 + y^{*2}_i} \, dt = \frac{_{ij}}{2} \\[2mm]
v^*_{v_{ij}} &= -\frac{1}{2} \int_0^{l_j} \frac{x^*_i - t}{(x^*_i - t)^2 + y^{*2}_i} \, dt = \frac{1}{2} \ln \frac{r_{i,j+1}}{r_{ij}}
\end{aligned}
\tag{4-42}
$$

where the definitions and special circumstances described for the source singularities are the same in the current case of distributed vortices.[*] In this case the vortex distribution induces an axial velocity on itself at the sheet, and no normal velocity.

Step 3. Flow tangency conditions to get N equations.

Our goal is to obtain a system of equations of the form:

$$\sum_{j=1}^{N} A_{ij} q_j + A_{i,N+1} = b_i \qquad i = 1,...N \tag{4-43}$$

which are solved for the unknown source and vortex strengths.

Recall the flow tangency condition was found to be:

$$-u_i \sin{}_i + v_i \cos{}_i = 0, \quad \text{for each } i, \quad i = 1,...N \tag{4-44}$$

---

[*] Note that Moran's Equation (4-88) has a sign error typo. The correct sign is used in Eq. (4-42) above.

where the velocities are given by:

$$u_i = V\cos\alpha + \sum_{j=1}^{N} q_j u_{s_{ij}} + \sum_{j=1}^{N} u_{v_{ij}}$$
$$v_i = V\sin\alpha + \sum_{j=1}^{N} q_j v_{s_{ij}} + \sum_{j=1}^{N} v_{v_{ij}}$$

(4-45)

Substituting into Eq. (4-45), the flow tangency equations, Eq. (4-44), above:

$$\left(-V\cos\alpha - \sum_{j=1}^{N} q_j u_{s_{ij}} - \sum_{j=1}^{N} u_{v_{ij}}\right)\sin\theta_i + \left(V\sin\alpha + \sum_{j=1}^{N} q_j v_{s_{ij}} + \sum_{j=1}^{N} v_{v_{ij}}\right)\cos\theta_i = 0$$

(4-46)

which is rewritten into:

$$\left[-V\sin\theta_i\cos\alpha + V\cos\theta_i\sin\alpha\right] - \sin\theta_i \sum_{j=1}^{N} q_j u_{s_{ij}} + \cos\theta_i \sum_{j=1}^{N} q_j v_{s_{ij}}$$
$$- \sin\theta_i \sum_{j=1}^{N} u_{v_{ij}} + \cos\theta_i \sum_{j=1}^{N} v_{v_{ij}} = 0$$

or

$$\underbrace{V\left(\cos\theta_i\sin\alpha - \sin\theta_i\cos\alpha\right)}_{-b_i} + \sum_{j=1}^{N}\underbrace{\left(\cos\theta_i v_{s_{ij}} - \sin\theta_i u_{s_{ij}}\right)q_j}_{A_{ij}}$$
$$+ \underbrace{\cos\theta_i \sum_{j=1}^{N} v_{v_{ij}} - \sin\theta_i \sum_{j=1}^{N} u_{v_{ij}}}_{A_{i,N+1}} = 0$$

(4-47)

Now get the formulas for A_{ij} and $A_{i,N+1}$ by replacing the formulas for $u_{s_{ij}}$, $v_{s_{ij}}$, $u_{v_{ij}}$, $v_{v_{ij}}$ with the ( )* values, where:

$$u = u^*\cos\theta_j - v^*\sin\theta_j$$
$$v = u^*\sin\theta_j + v^*\cos\theta_j$$

(4-48)

and we substitute into Eq. (4-47) for the values in A_{ij} and $A_{i,N+1}$ above.

Start with:

$$A_{ij} = \cos{}_i v_{s_{ij}} - \sin{}_i u_{s_{ij}}$$

$$= \cos{}_i\left(u_{s_{ij}}^* \sin{}_j + v_{s_{ij}}^* \cos{}_j\right) - \sin{}_i\left(u_{s_{ij}}^* \cos{}_j - v_{s_{ij}}^* \sin{}_j\right) \qquad (4\text{-}49)$$

$$= \left(\cos{}_i \sin{}_j - \sin{}_i \cos{}_j\right)u_{s_{ij}}^* + \left(\cos{}_i \cos{}_j - \sin{}_i \sin{}_j\right)v_{s_{ij}}^*$$

and we use trigonometric identities to combine terms into a more compact form. Operating on the first term in parenthesis:

$$\cos{}_i \sin{}_j = \frac{1}{2}\sin\left({}_i + {}_j\right) + \frac{1}{2}\sin\left(-\{{}_i - {}_j\}\right)$$

$$= \frac{1}{2}\sin\left({}_i + {}_j\right) - \frac{1}{2}\sin\left({}_i - {}_j\right) \qquad (4\text{-}50)$$

and

$$\sin{}_i \sin{}_j = \frac{1}{2}\sin\left({}_i + {}_j\right) + \frac{1}{2}\sin\left({}_i - {}_j\right) \qquad (4\text{-}51)$$

results in:

$$\left(\cos{}_i \sin{}_j - \sin{}_i \cos{}_j\right) = 0 - \sin\left({}_i - {}_j\right). \qquad (4\text{-}52)$$

Moving to the second term in parentheses above:

$$\cos{}_i \cos{}_j = \frac{1}{2}\cos\left({}_i + {}_j\right) + \frac{1}{2}\cos\left({}_i - {}_j\right)$$

$$\sin{}_i \sin{}_j = \frac{1}{2}\cos\left({}_i - {}_j\right) - \frac{1}{2}\cos\left({}_i + {}_j\right) \qquad (4\text{-}53)$$

and

$$\cos{}_i \cos{}_j + \sin{}_i \sin{}_j = \frac{1}{2}\cos\left({}_i + {}_j\right) + \frac{1}{2}\cos\left({}_i - {}_j\right) + \frac{1}{2}\cos\left({}_i - {}_j\right) - \frac{1}{2}\cos\left({}_i + {}_j\right)$$

$$= \cos\left({}_i - {}_j\right) \qquad (4\text{-}54)$$

so that the expression for A_{ij} can be written as:

$$A_{ij} = -\sin\left({}_i - {}_j\right)u_{s_{ij}}^* + \cos\left({}_i - {}_j\right)v_{s_{ij}}^* \qquad (4\text{-}55)$$

and using the definitions of

$$A_{ij} = \frac{1}{2}\sin({}_i - {}_j)\ln\frac{r_{i,j+1}}{r_{i,j}} + \frac{1}{2}\cos\left({}_i - {}_j\right){}_{ij}. \qquad (4\text{-}56)$$

Now look at the expression for b_i identified in (4-47):

$$b_i = V\left(\cos{}_i \sin - \sin{}_i \cos\right) \qquad (4\text{-}57)$$

where in the same fashion used above:

$$\cos\theta_i \sin\theta = \frac{1}{2}\sin(\theta_i + \theta) - \frac{1}{2}\sin(\theta_i - \theta)$$
$$\sin\theta_i \cos\theta = \frac{1}{2}\sin(\theta_i + \theta) + \frac{1}{2}\sin(\theta_i - \theta) \tag{4-58}$$

and

$$\cos\theta_i \sin\theta - \sin\theta_i \cos\theta = -\sin(\theta_i - \theta) \tag{4-59}$$

so that we get:

$$b_i = V_\infty \sin(\theta_i - \alpha). \tag{4-60}$$

Finally, work with the $A_{i,N+1}$ term:

$$\begin{aligned}
A_{i,N+1} &= \cos\theta_i \sum_{j=1}^{N} v_{v_{ij}} - \sin\theta_i \sum_{j=1}^{N} u_{v_{ij}} \\
&= \cos\theta_i \sum_{j=1}^{N}\left(u^*_{v_{ij}}\sin\theta_j + v^*_{v_{ij}}\cos\theta_j\right) - \sin\theta_i \sum_{j=1}^{N}\left(u^*_{v_{ij}}\cos\theta_j - v^*_{v_{ij}}\sin\theta_j\right) \\
&= \sum_{j=1}^{N}\left(\cos\theta_i \sin\theta_j u^*_{v_{ij}} + \cos\theta_i\cos\theta_j v^*_{v_{ij}} - \sin\theta_i\cos\theta_j u^*_{v_{ij}} + \sin\theta_i\sin\theta_j v^*_{v_{ij}}\right) \\
&= \sum_{j=1}^{N}\underbrace{\left(\cos\theta_i\cos\theta_j + \sin\theta_i\sin\theta_j\right)}_{a}v^*_{v_{ij}} + \underbrace{\left(\cos\theta_i\sin\theta_j - \sin\theta_i\cos\theta_j\right)}_{b}u^*_{v_{ij}}
\end{aligned} \tag{4-61}$$

and a and b can be simplified to:

$$a = \cos(\theta_i - \theta_j)$$
$$b = -\sin(\theta_i - \theta_j). \tag{4-62}$$

Substituting for a and b in the above equation:

$$A_{i,N+1} = \sum_{j=1}^{N}\left\{\cos(\theta_i - \theta_j)v^*_{v_{ij}} - \sin(\theta_i - \theta_j)u^*_{v_{ij}}\right\} \tag{4-63}$$

and using the definition of we arrive at the final result:

$$A_{i,N+1} = \frac{1}{2}\sum_{j=1}^{N}\cos(\theta_i - \theta_j)\ln\frac{r_{i,j+1}}{r_{i,j}} - \sin(\theta_i - \theta_j)\beta_{ij}. \tag{4-64}$$

To sum up (repeating the results found above), the equations for the A_{ij}, $A_{i,N+1}$, and b_i are given by (4-56), (4-64), and (4-60):

$$A_{ij} = \frac{1}{2}\sin(\theta_i - \theta_j)\ln\frac{r_{i,j+1}}{r_{i,j}} + \frac{1}{2}\cos\left(\theta_i - \theta_j\right)\beta_{ij}$$

$$A_{i,N+1} = \frac{1}{2}\sum_{j=1}^{N}\cos(\theta_i - \theta_j)\ln\frac{r_{i,j+1}}{r_{i,j}} - \sin(\theta_i - \theta_j)\beta_{ij}$$

$$b_i = V\sin(\theta_i - \alpha)$$

Step 4. Kutta Condition to get equation N+1

To complete the system of $N+1$ equations, we use the Kutta condition, which we previously defined as:

$$u_1 \cos\theta_1 + v_1\sin\theta_1 = -u_N\cos\theta_N - v_N\sin\theta_N \tag{4-66}$$

and substitute into this expression the formulas for the velocities due to the freestream and singularities given in equation (4-31). In this case they are written as:

$$
\begin{aligned}
u_1 &= V\cos\alpha + \sum_{j=1}^{N} q_j u_{s_{1j}} + \sum_{j=1}^{N} u_{v_{1j}}\\[4pt]
v_1 &= V\sin\alpha + \sum_{j=1}^{N} q_j v_{s_{1j}} + \sum_{j=1}^{N} v_{v_{1j}}\\[4pt]
u_N &= V\cos\alpha + \sum_{j=1}^{N} q_j u_{s_{Nj}} + \sum_{j=1}^{N} u_{v_{Nj}}\\[4pt]
v_N &= V\sin\alpha + \sum_{j=1}^{N} q_j v_{s_{Nj}} + \sum_{j=1}^{N} v_{v_{Nj}}
\end{aligned}
\tag{4-67}
$$

Substituting into the Kutta condition equation we obtain:

2/24/98

$$V \cos \; + \sum_{j=1}^{N} q_j u_{s_{1j}} + \sum_{j=1}^{N} u_{v_{1j}} \cos {}_1$$

$$+ \; V \sin \; + \sum_{j=1}^{N} q_j v_{s_{1j}} + \sum_{j=1}^{N} v_{v_{1j}} \sin {}_1$$

$$+ \; V \cos \; + \sum_{j=1}^{N} q_j u_{s_{Nj}} + \sum_{j=1}^{N} u_{v_{Nj}} \cos {}_N$$

$$+ \; V \sin \; + \sum_{j=1}^{N} q_j v_{s_{Nj}} + \sum_{j=1}^{N} v_{v_{Nj}} \sin {}_N = 0$$

(4-68)

and our goal will be to manipulate this expression into the form:

$$\sum_{j=1}^{N} A_{N+1,j} q_j + A_{N+1,N+1} = b_{N+1}$$

(4-69)

which is the $N + 1^{st}$ equation which completes the system for the $N + 1$ unknowns.

Start by regrouping terms in the above equation to write it in the form:

$$\sum_{j=1}^{N} \underbrace{\left(u_{s_{1j}} \cos {}_1 + v_{s_{1j}} \sin {}_1 + u_{s_{Nj}} \cos {}_N + v_{s_{Nj}} \sin {}_N \right)}_{A_{N+1,j}} q_j$$

$$+ \underbrace{\sum_{j=1}^{N} \left(u_{v_{1j}} \cos {}_1 + v_{v_{1j}} \sin {}_1 + u_{v_{Nj}} \cos {}_N + v_{v_{Nj}} \sin {}_N \right)}_{A_{N+1,N+1}}$$

$$= \underbrace{-\left(V \cos \cos {}_1 + V \sin \sin {}_1 + V \cos \cos {}_N + V \sin \sin {}_N \right)}_{b_{N+1}} \quad . $$

(4-70)

Obtain the final expression for b_{N+1} first:

$$b_{N+1} = -V \left(\underbrace{\cos \cos {}_1 + \sin \sin {}_1}_{\cos\left(- {}_1\right)} + \underbrace{\cos \cos {}_N + \sin \sin {}_N}_{\cos\left(- {}_N\right)} \right)$$

(4-71)

and using the trigonometric identities to obtain the expression for b_{N+1}:

$$b_{N+1} = -V \cos\left({}_1 - \right) - V \cos\left({}_N - \right)$$

(4-72)

where we made use of $\cos(-A) = \cos A$.

Now work with $A_{N+1,j}$:

$$A_{N+1,j} = u_{s_{1j}} \cos\theta_1 + v_{s_{1j}} \sin\theta_1 + u_{s_{Nj}} \cos\theta_N + v_{s_{Nj}} \sin\theta_N \qquad (4\text{-}73)$$

and replace the influence coefficients with their related $(\ )^*$ values:

$$
\begin{aligned}
u_{s_{1j}} &= u^*_{s_{1j}} \cos\theta_j - v^*_{s_{1j}} \sin\theta_j \\
v_{s_{1j}} &= u^*_{s_{1j}} \sin\theta_j + v^*_{s_{1j}} \cos\theta_j \\
u_{s_{Nj}} &= u^*_{s_{Nj}} \cos\theta_j - v^*_{s_{Nj}} \sin\theta_j \\
v_{s_{Nj}} &= u^*_{s_{Nj}} \sin\theta_j + v^*_{s_{Nj}} \cos\theta_j
\end{aligned}
\qquad (4\text{-}74)
$$

so that we can write:

$$
\begin{aligned}
A_{N+1,j} = {} & \left(u^*_{s_{1j}} \cos\theta_j - v^*_{s_{1j}} \sin\theta_j \right)\cos\theta_1 \\
& + \left(u^*_{s_{1j}} \sin\theta_j + v^*_{s_{1j}} \cos\theta_j \right)\sin\theta_1 \\
& + \left(u^*_{s_{Nj}} \cos\theta_j - v^*_{s_{Nj}} \sin\theta_j \right)\cos\theta_N \\
& + \left(u^*_{s_{Nj}} \sin\theta_j + v^*_{s_{Nj}} \cos\theta_j \right)\sin\theta_N
\end{aligned}
\qquad (4\text{-}75)
$$

or:

$$
\begin{aligned}
A_{N+1,j} = {} & \left(\cos\theta_j \cos\theta_1 + \sin\theta_j \sin\theta_1 \right) u^*_{s_{1j}} \\
& + \left(\cos\theta_j \cos\theta_N + \sin\theta_j \sin\theta_N \right) u^*_{s_{Nj}} \\
& + \left(\cos\theta_j \sin\theta_1 - \sin\theta_j \cos\theta_1 \right) v^*_{s_{1j}} \\
& + \left(\cos\theta_j \sin\theta_N - \sin\theta_j \cos\theta_N \right) v^*_{s_{Nj}}
\end{aligned}
\qquad (4\text{-}76)
$$

Use the following trig relations to simplify the equation:

$$
\begin{aligned}
\cos\theta_j \cos\theta_1 + \sin\theta_j \sin\theta_1 &= \cos\left(\theta_j - \theta_1\right) \\
\cos\theta_j \cos\theta_N + \sin\theta_j \sin\theta_N &= \cos\left(\theta_j - \theta_N\right) \\
\cos\theta_j \sin\theta_1 - \sin\theta_j \cos\theta_1 &= -\sin\left(\theta_j - \theta_1\right) \\
\cos\theta_j \sin\theta_N - \sin\theta_j \cos\theta_N &= -\sin\left(\theta_j - \theta_N\right)
\end{aligned}
\qquad (4\text{-}77)
$$

and substitute into Eq. (4-76) to obtain:

$$A_{N+1,j} = \cos\left(\theta_j - \theta_1\right)u^*_{s_{1j}} + \cos\left(\theta_j - \theta_N\right)u^*_{s_{Nj}}$$
$$- \sin\left(\theta_j - \theta_1\right)v^*_{s_{1j}} - \sin\left(\theta_j - \theta_N\right)v^*_{s_{Nj}} .$$

(4-78)

Use the definition of the influence coefficients:

$$u^*_{s_{1j}} = -\frac{1}{2}\ln\frac{r_{1,j+1}}{r_{1,j}} \qquad u^*_{s_{Nj}} = -\frac{1}{2}\ln\frac{r_{N,j+1}}{r_{N,j}}$$

$$v^*_{s_{1j}} = \frac{\beta_{1,j}}{2} \qquad v^*_{s_{Nj}} = \frac{\beta_{N,j}}{2}$$

(4-79)

to write the equation for $A_{N+1,}$:

$$A_{N+1,j} = -\frac{\cos\left(\theta_j - \theta_1\right)}{2}\ln\frac{r_{1,j+1}}{r_{1,j}} - \frac{\cos\left(\theta_j - \theta_N\right)}{2}\ln\frac{r_{N,j+1}}{r_{N,j}}$$
$$- \frac{\sin\left(\theta_j - \theta_1\right)}{2}\beta_{1,j} - \frac{\sin\left(\theta_j - \theta_N\right)}{2}\beta_{N,j} .$$

(4-80)

Finally, use symmetry and odd/even relations to write down the final form:

$$A_{N+1,j} = \frac{1}{2}\begin{array}{c} \sin(\theta_1 - \theta_j)\,\beta_{1,j} + \sin(\theta_N - \theta_j)\,\beta_{N,j} \\[6pt] -\cos(\theta_1 - \theta_j)\ln\frac{r_{1,j+1}}{r_{1,j}} - \cos(\theta_N - \theta_j)\ln\frac{r_{N,j+1}}{r_{N,j}} \end{array} .$$

(4-81)

Now work with $A_{N+1,N+1}$:

$$A_{N+1,N+1} = \sum_{j=1}^{N}\left(u_{v_{1j}}\cos\theta_1 + v_{v_{1j}}\sin\theta_1 + u_{v_{Nj}}\cos\theta_N + v_{v_{Nj}}\sin\theta_N\right)$$

(4-82)

where we substitute in for the ( )* coordinate system, Eq. (4-32), and obtain:

$$A_{N+1,N+1} = \sum_{j=1}^{N}\begin{array}{c}\left(u^*_{v_{1j}}\cos\theta_j - v^*_{v_{1j}}\sin\theta_j\right)\cos\theta_1 + \left(u^*_{v_{1j}}\sin\theta_j + v^*_{v_{1j}}\cos\theta_j\right)\sin\theta_1 \\[6pt] +\left(u^*_{v_{Nj}}\cos\theta_j - v^*_{v_{Nj}}\sin\theta_j\right)\cos\theta_N + \left(u^*_{v_{Nj}}\sin\theta_j + v^*_{v_{Nj}}\cos\theta_j\right)\sin\theta_N\end{array}$$

(4-83)

or:

$$A_{N+1,N+1} = \sum_{j=1}^{N} \underbrace{(\cos\theta_j \cos\theta_1 + \sin\theta_j \sin\theta_1)}_{\cos(\theta_j - \theta_1)} u^*_{v_{1j}} + \underbrace{(\cos\theta_j \sin\theta_1 - \sin\theta_j \cos\theta_1)}_{-\sin(\theta_j - \theta_1)} v^*_{v_{1j}} + \underbrace{(\cos\theta_j \cos\theta_N + \sin\theta_j \sin\theta_N)}_{\cos(\theta_j - \theta_N)} u^*_{v_{Nj}} + \underbrace{(\cos\theta_j \sin\theta_N - \sin\theta_j \cos\theta_N)}_{-\sin(\theta_j - \theta_N)} v^*_{v_{Nj}}$$

(4-84)

which is:

$$A_{N+1,N+1} = \sum_{j=1}^{N} \begin{array}{l} \cos(\theta_j - \theta_1) u^*_{v_{1j}} - \sin(\theta_j - \theta_1) v^*_{v_{1j}} \\ + \cos(\theta_j - \theta_N) u^*_{v_{Nj}} - \sin(\theta_j - \theta_N) v^*_{v_{Nj}} \end{array} \quad ,$$

and using odd/even trig relations we get the form given by Moran[6]:

$$A_{N+1,N+1} = \sum_{j=1}^{N} \begin{array}{l} \sin(\theta_1 - \theta_j) v^*_{v_{1j}} + \sin(\theta_N - \theta_j) v^*_{v_{Nj}} \\ + \cos(\theta_1 - \theta_j) u^*_{v_{1j}} + \cos(\theta_N - \theta_j) u^*_{v_{Nj}} \end{array} \quad .$$

(4-86)

We now substitute the formulas derived above for the influence coefficients given in Eq. (4-42). The final equation is:

$$A_{N+1,N+1} = \frac{1}{2} \sum_{j=1}^{N} \begin{array}{l} \sin\left(\theta_1 - \theta_j\right) \ln \frac{r_{1,j+1}}{r_{i,j}} + \sin\left(\theta_N - \theta_j\right) \ln \frac{r_{N,j+1}}{r_{N,j}} \\ + \cos(\theta_1 - \theta_j) \beta_{1,j} + \cos(\theta_N - \theta_j) \beta_{N,j} \end{array} \quad .$$

(4-86)

After substituting in the values of the velocities in terms of the singularity strengths, and performing some algebraic manipulation, a form of the coefficients suitable for computations is obtained.

The final equations associated with the Kutta condition are:

$$A_{N+1,j} = \frac{1}{2} \begin{array}{l} \sin(\theta_1 - \theta_j) \beta_{1,j} + \sin(\theta_N - \theta_j) \beta_{N,j} \\ -\cos(\theta_1 - \theta_j) \ln \frac{r_{1,j+1}}{r_{1,j}} - \cos(\theta_N - \theta_j) \ln \frac{r_{N,j+1}}{r_{N,j}} \end{array}$$

(4-81)

$$A_{N+1,N+1} = \frac{1}{2} \sum_{j=1}^{N} \begin{array}{l} \sin\left(\theta_1 - \theta_j\right) \ln \frac{r_{1,j+1}}{r_{i,j}} + \sin\left(\theta_N - \theta_j\right) \ln \frac{r_{N,j+1}}{r_{N,j}} \\ + \cos(\theta_1 - \theta_j) \beta_{1,j} + \cos(\theta_N - \theta_j) \beta_{N,j} \end{array}$$

(4-86)

$$b_{N+1} = -V \cos(\theta_1 - \alpha) - V \cos(\theta_N - \alpha).$$

(4-72)

Step 5. Solve the system for q_i, .

The coefficients derived above provide the required coefficients to solve a system of linear algebraic equations for the $N+1$ unknowns, q_i, $i = 1,...,N$ and given by (4-43) and (4-69):

$$\sum_{j=1}^{N} A_{ij}q_j + A_{i,N+1} \quad = b_i \qquad\qquad i = 1,...N$$

$$\sum_{j=1}^{N} A_{N+1,j}q_j + A_{N+1,N+1} \quad = b_{N+1}$$

(4-87)

This is easily done using any number of computer subroutines.

Step 6. Given q_i, and , write down the equations for the tangential velocity at each panel control point.

At each control point, $(v_n = 0)$, find u_t, the tangential velocity starting with:

$$u_{t_i} = u_i \cos{}_i + v_i \sin{}_i$$

$$= V \cos{} + \sum_{j=1}^{N} u_{s_{ij}}q_j + \sum_{j=1}^{N} u_{v_{ij}} \quad \cos{}_i .$$

(4-88)

$$+ V \sin{} + \sum_{j=1}^{N} v_{s_{ij}}q_j + \sum_{j=1}^{N} v_{v_{ij}} \quad \sin{}_i$$

Using the ( )* values of the influence coefficients,

$$u_{t_i} = V \cos{} + \sum_{j=1}^{N} \left(u^*_{s_{ij}} \cos{}_j - v^*_{s_{ij}} \sin{}_j \right) q_j + \sum_{j=1}^{N} \left(u^*_{v_{ij}} \cos{}_j - v^*_{v_{ij}} \sin{}_j \right) \cos{}_i$$

$$+ V \sin{} + \sum_{j=1}^{N} \left(u^*_{s_{ij}} \sin{}_j + v^*_{s_{ij}} \cos{}_j \right) q_j + \sum_{j=1}^{N} \left(u^*_{v_{ij}} \sin{}_j + v^*_{v_{ij}} \cos{}_j \right) \sin{}_i$$

(4-89)

or:

$$u_{t_i} = V \cos \ \cos \ _i + V \sin \ \sin \ _i$$

$$+ \sum_{j=1}^{N} \left\{ u^{*}_{s_{ij}} \cos \ _j \cos \ _i - v^{*}_{s_{ij}} \sin \ _j \cos \ _i + u^{*}_{s_{ij}} \sin \ _j \sin \ _i + v^{*}_{s_{ij}} \cos \ _j \sin \ _i \right\} q_j \ .$$

$$+ \sum_{j=1}^{N} \left\{ u^{*}_{v_{ij}} \cos \ _j \cos \ _i - v^{*}_{v_{ij}} \sin \ _j \cos \ _i + u^{*}_{v_{ij}} \sin \ _j \sin \ _i + v^{*}_{s_{ij}} \cos \ _j \sin \ _i \right\}$$

(4-90)

Collecting terms:

$$u_{t_i} = \underbrace{(\cos \ \cos \ _i + \sin \ \sin \ _i)}_{\cos(\ - \ _i)} V$$

$$+ \sum_{j=1}^{N} \underbrace{(\cos \ _j \cos \ _i + \sin \ _j \sin \ _i)}_{\cos(\ _j - \ _i)} u^{*}_{s_{ij}} + \underbrace{(\cos \ _j \sin \ _i - \sin \ _j \cos \ _i)}_{-\sin(\ _j - \ _i)} v^{*}_{s_{ij}} \ q_j \quad (4\text{-}91)$$

$$+ \sum_{j=1}^{N} \underbrace{(\cos \ _j \cos \ _i + \sin \ _j \sin \ _i)}_{\cos(\ _j - \ _i)} u^{*}_{v_{ij}} + \underbrace{(\cos \ _j \sin \ _i - \sin \ _j \cos \ _i)}_{-\sin(\ _j - \ _i)} v^{*}_{v_{ij}}$$

which becomes:

$$u_{t_i} = \cos(\ - \ _i) V + \sum_{j=1}^{N} \left\{ \cos(\ _j - \ _i) u^{*}_{s_{ij}} - \sin(\ _j - \ _i) v^{*}_{s_{ij}} \right\} q_j$$

$$+ \sum_{j=1}^{N} \left\{ \cos(\ _j - \ _i) u^{*}_{v_{ij}} - \sin(\ _j - \ _i) v^{*}_{v_{ij}} \right\} \quad . \quad (4\text{-}92)$$

Using the definitions of the ( )* influence coefficients, and some trigonometric identities, we obtain the final result:

$$u_{t_i} = \cos(\ _i - \ ) V + \sum_{j=1}^{N} \frac{q_i}{2} \ \sin(\ _i - \ _j) \ _{ij} - \cos(\ _i - \ _j) \ln \frac{r_{i,j+1}}{r_{i,j}}$$

$$+ \frac{1}{2} \sum_{j=1}^{N} \sin(\ _i - \ _j) \ln \frac{r_{i,j+1}}{r_{i,j}} + \cos(\ _i - \ _j) \ _{ij} \quad . \quad (4\text{-}93)$$

Step 7. Finally, the surface pressure coefficient can be found from:

$$C_{P_i} = 1 - \left(\frac{u_{t_i}}{V}\right)^2 \qquad (4\text{-}94)$$

using u_i from Eq. (4-93).

This completes our derivation of one panel method scheme in two dimensions. Imagine the difficulty in performing the algebra required to extend this approach to three dimensions! That's why we've used a two-dimensional example.

4.5 Program PANEL

Program **PANEL** is an exact implementation of the analysis given in Section 4.4, and is essentially the program given by Moran.[6] Other panel method programs are available in the textbooks by Houghton and Carpenter,[10] and Kuethe and Chow.[11] Moran's program includes a subroutine to generate the ordinates for the NACA 4-digit and 5-digit airfoils (see Appendix A for a description of these airfoil sections). The main drawback is the requirement for a trailing edge thickness that's exactly zero. To accommodate this restriction, the ordinates generated internally have been altered slightly from the official ordinates. The extension of the program to handle arbitrary airfoils is an exercise. The freestream velocity in **PANEL** is assumed to be unity, since the inviscid solution in coefficient form is independent of scale.

PANEL's node points are distributed employing the widely used cosine spacing function. The equation for this spacing is given by defining the points on the thickness distribution to be placed at:

$$\frac{x_i}{c} = \frac{1}{2}\left[1 - \cos\left(\frac{(i-1)}{(N-1)}\right)\right] \qquad i = 1,...,N. \qquad (4\text{-}95)$$

These locations are then altered when camber is added (see Eqns. (A-1) and (A-2) in App. A). This approach is used to provide a smoothly varying distribution of panel node points which concentrate points around the leading and trailing edges.

An example of the accuracy of program **PANEL** is given in Fig. 4-11, where the results from **PANEL** for the NACA 4412 airfoil are compared with results obtained from an exact conformal mapping of the airfoil (comments on the mapping methods are given in Chapter 9 on Geometry and Grids. Conformal transformations can also be used to generate meshes of points for use in field methods). The agreement is nearly perfect.

Numerical studies need to be conducted to determine how many panels are required to obtain accurate results. Both forces and moments and pressure distributions should be examined.
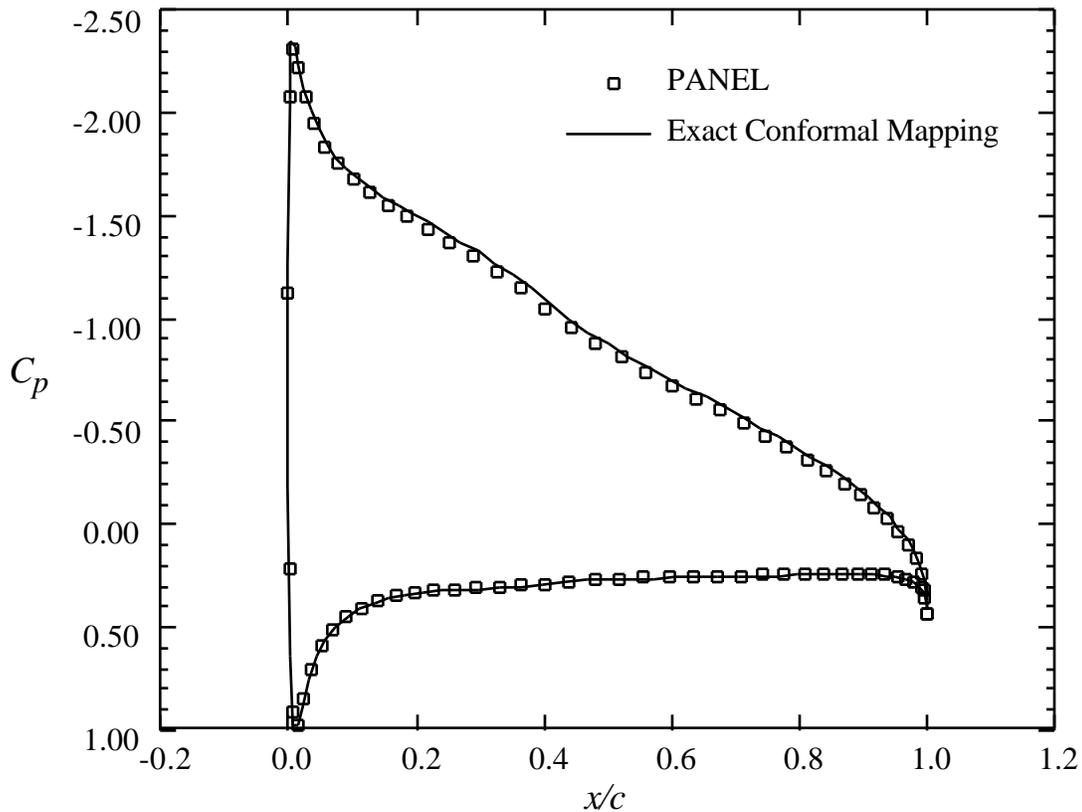
Figure 4-11. Comparison of results from program **PANEL** with an essentially exact
mapping solution for the NACA 4412 airfoil at 6° angle-of-attack.

You can select the number of panels used to represent the surface. How many should you use? Most computational programs provide the user with freedom to decide how detailed (expensive - in dollars or time) the calculations should be. One of the first things the user should do is evaluate how detailed the calculation should be to obtain the level of accuracy desired. In the **PANEL** code your control is through the number of panels used.

We check the sensitivity of the solution to the number of panels by comparing force and moment results and pressure distributions with increasing numbers of panels. This is done using two different methods. Figures 4-12 and 4-13 present the change of drag and lift, respectively, using the first method. For **PANEL**, which uses an inviscid incompressible flowfield model, the drag should be exactly zero. The drag coefficient found by integrating the pressures over the airfoil is an indication of the error in the numerical scheme. The drag obtained using a surface (or "nearfield") pressure integration is a numerically sensitive calculation, and is a strict test of the method. The figures show the drag going to zero, and the lift becoming constant as the number of

panels increase. In this style of presentation it is hard to see exactly how quickly the solution is converging to a fixed value.

The results given in Figures 4-12 and 4-13 indicate that 60-80 panels (30 upper, 30 lower for example) should be enough panels. Note that the lift is presented in an extremely expanded scale. Drag also uses an expanded scale. Because drag is typically a small number, it is frequently described in drag counts, where 1 drag count is a C_D of 0.0001.

To estimate the limit for an infinitely large number of panels the results can be plotted as a function of the reciprocal of the number of panels. Thus the limit result occurs as $1/n$ goes to zero. Figures 4-14, 4-15, and 4-16 present the results in this manner for the case given above, and with the pitching moment included for examination in the analysis.
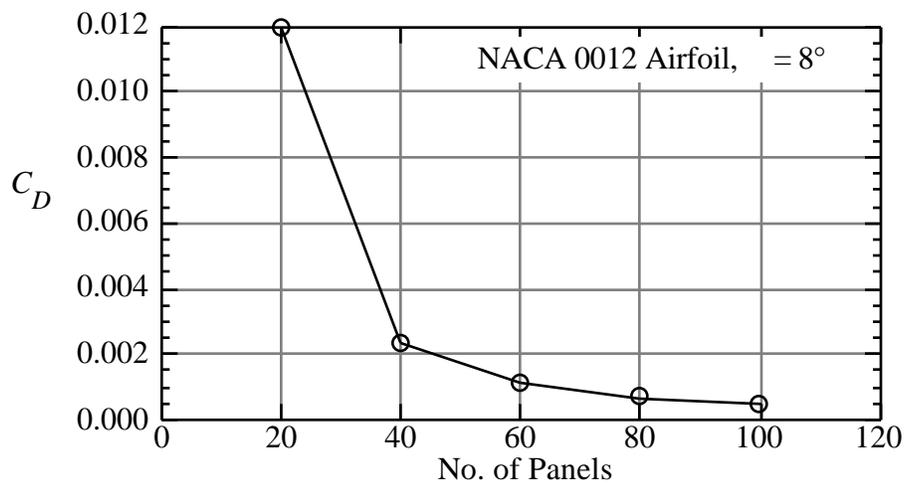
Figure 4-12. Change of drag with number of panels.
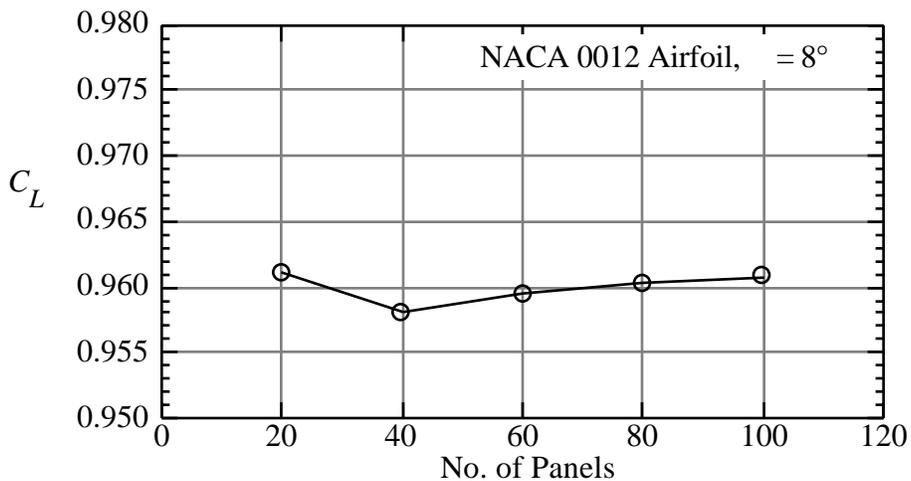
Figure 4-13. Change of lift with number of panels.
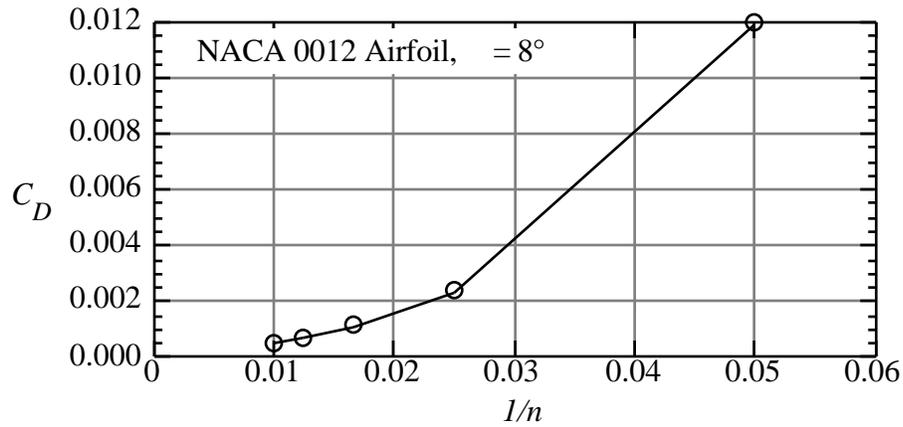
Figure 4-14. Change of drag with the inverse of the number of panels.
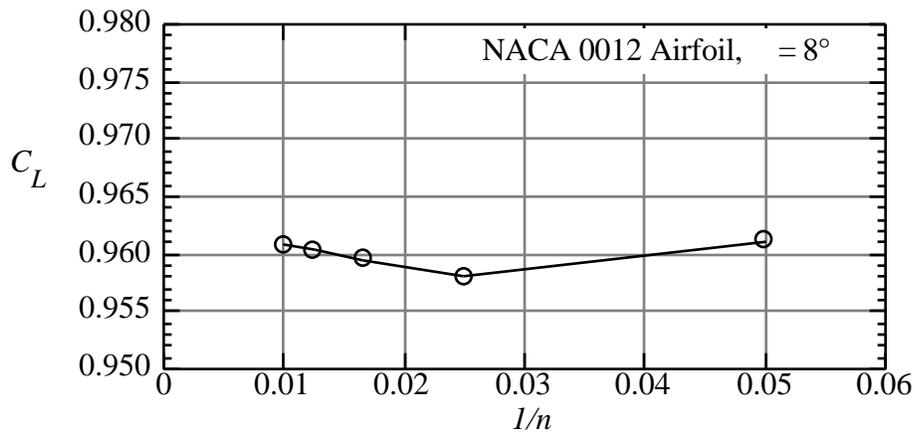
Figure 4-15. Change of lift with the inverse of the number of panels.
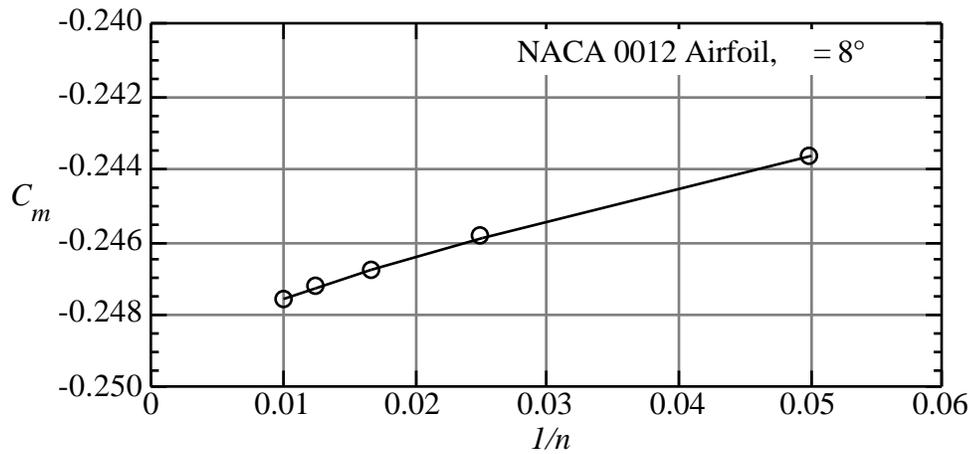
Figure 4-16. Change of pitching moment with the inverse of the number of panels.

The results given in Figures 4-14 through 4-16 show that the program **PANEL** produces results that are relatively insensitive to the number of panels once fifty or sixty panels are used, and by extrapolating to $1/n = 0$ an estimate of the limiting value can be obtained.

In addition to forces and moments, the sensitivity of the pressure distributions to changes in panel density should also be investigated. Pressure distributions are shown in Figures 4-17, 4-18, and 4-19. The case for 20 panels is given in Figure 4-17. Although the character of the pressure distribution is emerging, it's clear that more panels are required to define the details of the pressure distribution. The stagnation pressure region on the lower surface of the leading edge is not yet distinct. The expansion peak and trailing edge recovery pressure are also not resolved clearly. Figure 4-18 contains a comparison between 20 and 60 panel cases. In this case it appears that the pressure distribution is well defined with 60 panels. This is confirmed in Figure 4-19, which demonstrates that it is almost impossible to identify the differences between the 60 and 100 panel cases. This type of study should (and in fact *must*) be conducted when using computational aerodynamics methods.
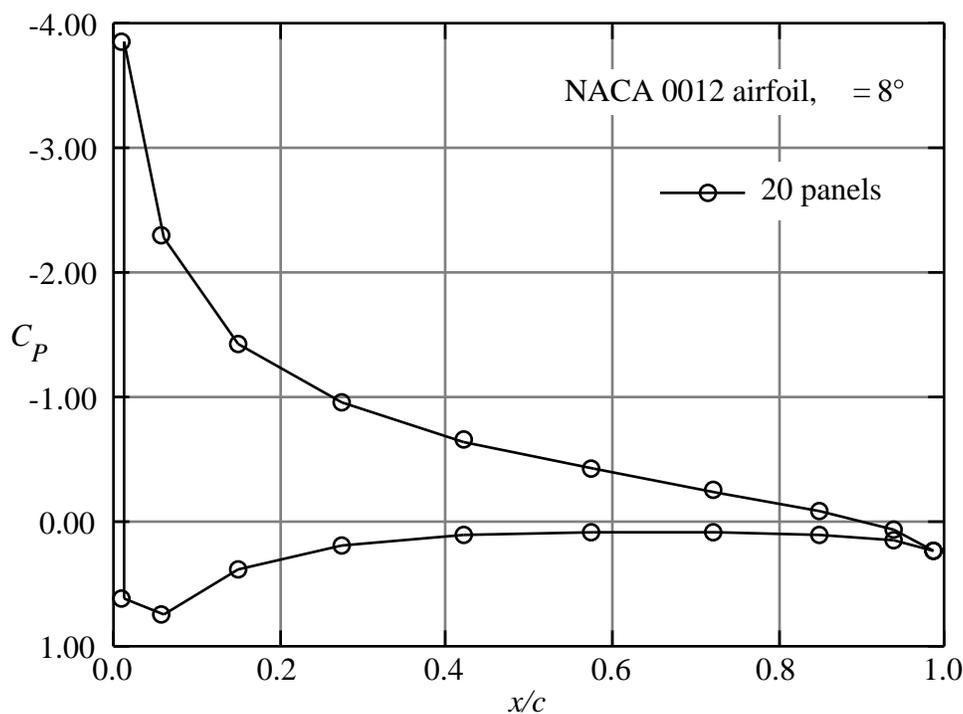
Figure 4-17. Pressure distribution from progrm PANEL, 20 panels.
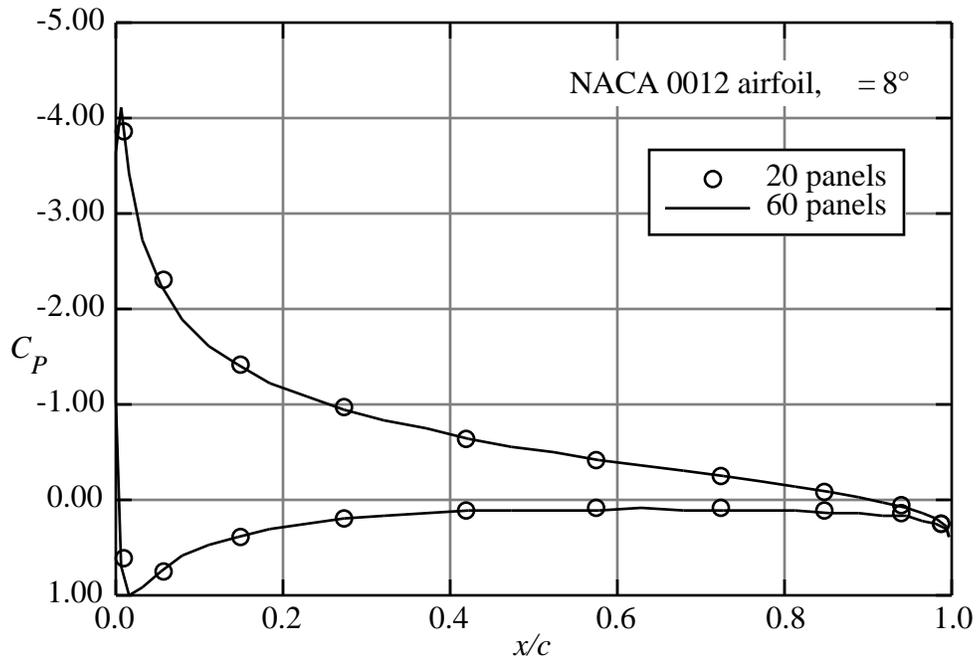
Figure 4-18. Pressure distribution from progrm PANEL,
comparing results using 20 and 60 panels.
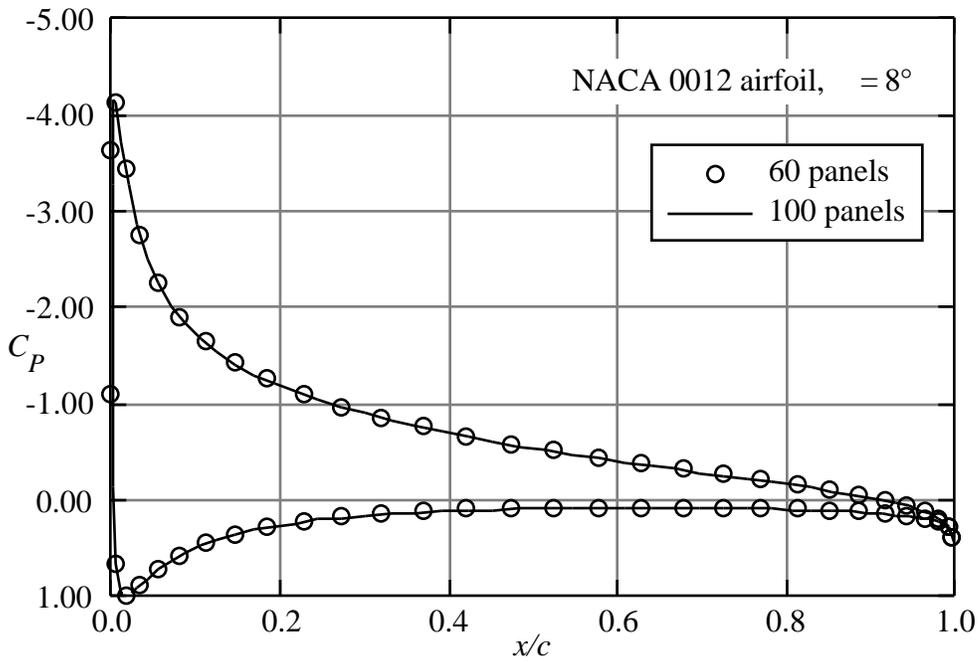
Figure 4-19. Pressure distribution from progrm PANEL,
comparing results using 60 and 100 panels.

Having examined the convergence of the mathematical solution, we investigate the agreement with experimental data. Figure 4-20 compares the lift coefficients from the inviscid solutions obtained from **PANEL** with experimental data from Abbott and von Doenhof.[12] Agreement is good at low angles of attack, where the flow is fully attached. The agreement deteriorates as the angle of attack increases, and viscous effects start to show up as a reduction in lift with increasing angle of attack, until, finally, the airfoil stalls. The inviscid solutions from **PANEL** cannot capture this part of the physics. The difference in the airfoil behavior at stall between the cambered and uncambered airfoil will be discussed further in Chapter 10. Essentially, the differences arise due to different flow separation locations on the different airfoils. The cambered airfoil separates at the trailing edge first. Stall occurs gradually as the separation point moves forward on the airfoil with increasing incidence. The uncambered airfoil stalls due to a sudden separation at the leading edge. An examination of the difference in pressure distributions to be discussed next can be studied to see why this might be the case.
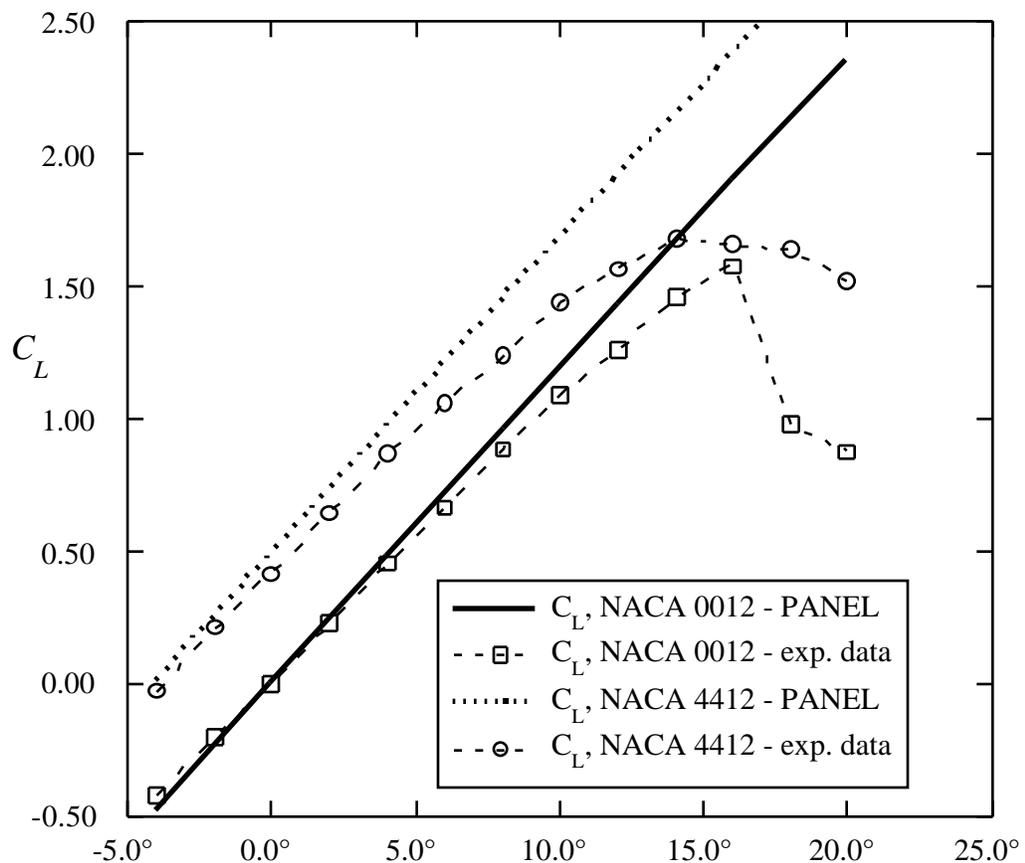
Figure 4-20. Comparison of PANEL lift predictions with experimental data, (Ref. 12).

The pitching moment characteristics are also important. Figure 4-21 provides a comparison of the **PANEL** pitching moment predictions (about the quarter chord point) with experimental data. In this case the calculations indicate that the computed location of the aerodynamic center, $dC_m / dC_L = 0$, is not exactly at the quarter chord, although the experimental data is very close to this value. The uncambered NACA 0012 data shows nearly zero pitching moment until flow separation starts to occur. The cambered airfoil shows a significant pitching moment, and a trend due to viscous effects that is exactly opposite the computed prediction.
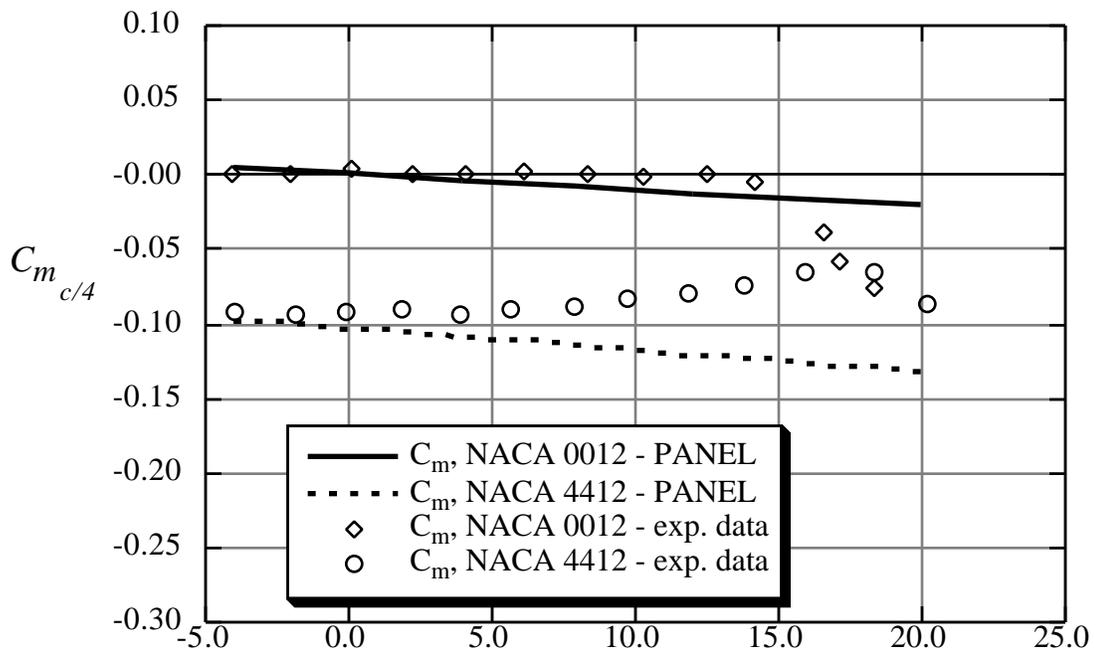
Figure 4-21. Comparison of PANEL moment predictions with experimental data, (Ref. 12).

We do not compare the drag prediction from **PANEL** with experimental data. In two-dimensional incompressible inviscid flow the drag is zero. In the actual case, drag arises from skin friction effects, further additional form drag due to the small change of pressure on the body due to the boundary layer (which primarily prevents full pressure recovery at the trailing edge), and drag due to increasing viscous effects with increasing angle of attack. A well designed airfoil will have a drag value very nearly equal to the skin friction and nearly invariant with incidence until the maximum lift coefficient is approached.

In addition to the force and moment comparisons, we need to compare the pressure distributions predicted with PANEL to experimental data. Figure 4-22 provides one example. The NACA 4412 experimental pressure distribution is compared with **PANEL** predictions. In general

the agreement is very good. The primary area of disagreement is at the trailing edge. Here viscous effects act to prevent the recovery of the experimental pressure to the levels predicted by the inviscid solution. The disagreement on the lower surface is surprising, and suggests that the angle of attack from the experiment is not precise.
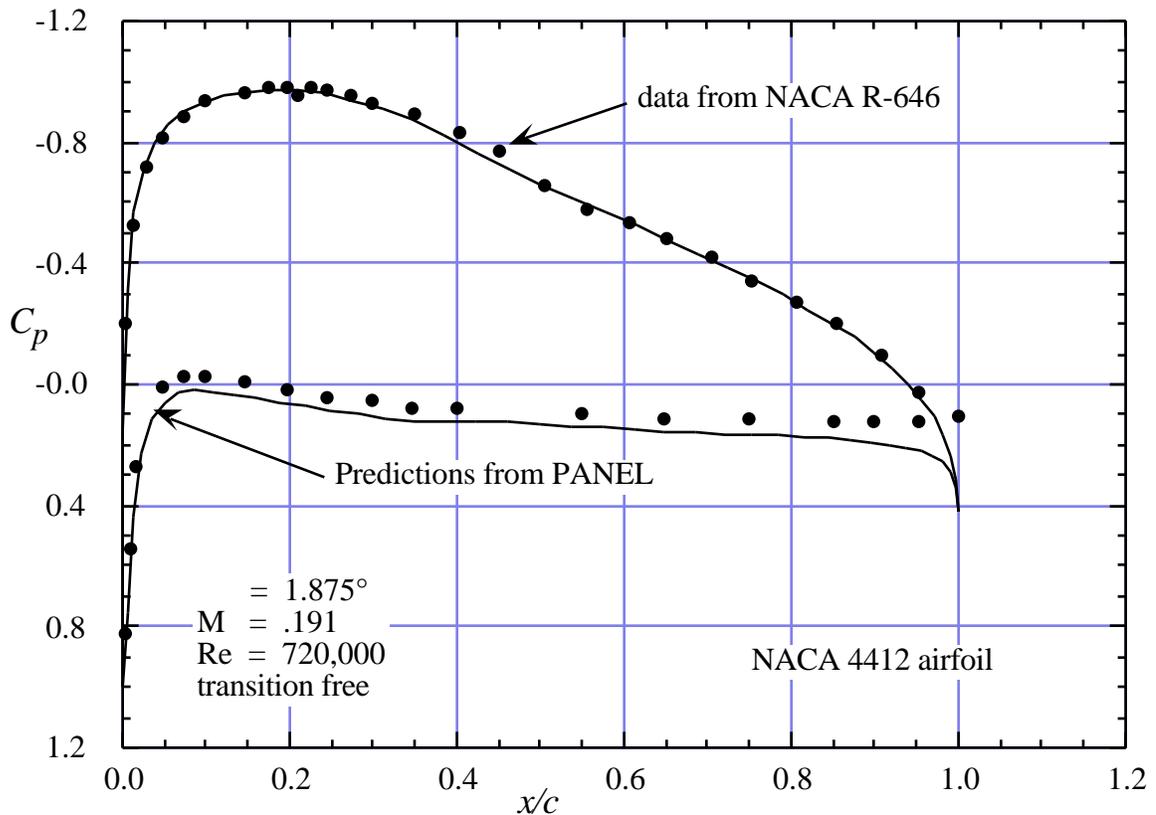
Figure 4-22. Comparison of pressure distribution from PANEL with data.

Panel methods often have trouble with accuracy at the trailing edge of airfoils with cusped trailing edges, so that the included angle at the trailing edge is zero. Figure 4-23 shows the predictions of program **PANEL** compared with an exact mapping solution (**FLO36** run at low Mach number, see Chap. 11) for two cases. Figure 4-23a is for a case with a small trailing edge angle: the NACA 651-012, while Fig. 4-23b is for the more standard 6A version of the airfoil. The corresponding airfoil shapes are shown Fig. 4-24.

a. 6-series, cusped TE

b. 6A-series, finite TE angle
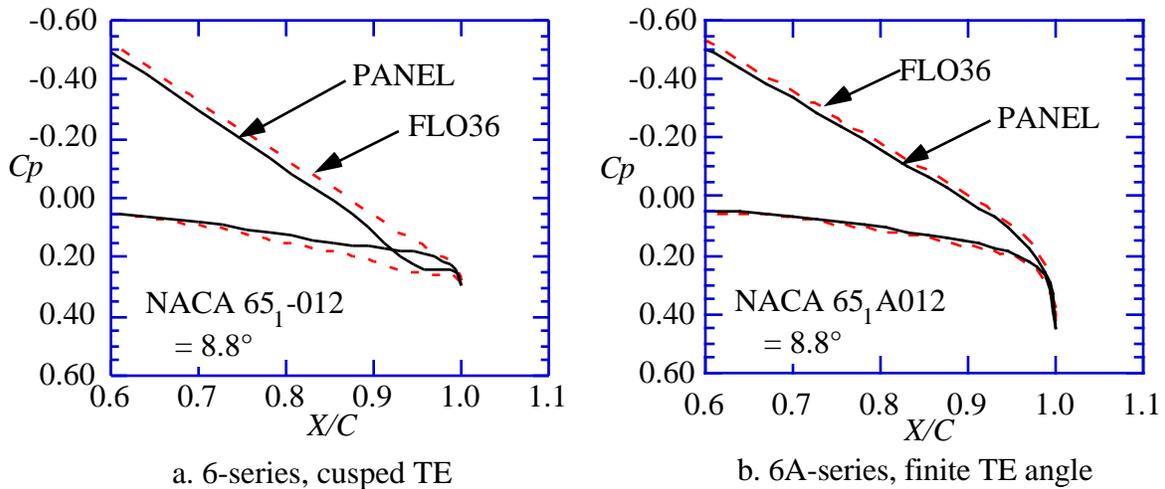
Figure 23. **PANEL** Performance near the airfoil trailing edge
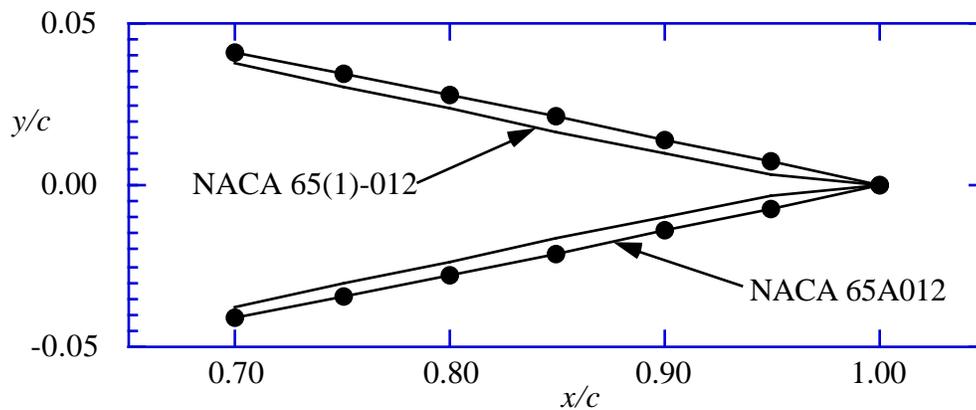
Figure 4-24. Comparison at the trailing edge of 6- and 6A-series airfoil geometries.

This case demonstrates a situation where this particular panel method is not accurate. Is this a practical consideration? Yes and no. The 6-series airfoils were theoretically derived by specifying a pressure distribution and determining the required shape. The small trailing edge angles (less than half those of the 4-digit series), cusped shape, and the unobtainable zero thickness specified at the trailing edge resulted in objections from the aircraft industry. These airfoils were very difficult to use on operational aircraft. Subsequently, the 6A-series airfoils were introduced to remedy the problem. These airfoils had larger trailing edge angles (approximately the same as the 4-digit series), and were made up of nearly straight (or flat) surfaces over the last 20% of the airfoil. Most applications of 6-series airfoils today actually use the modified 6A-series thickness distribution. This is an area where the user should check the performance of a particular panel method.

4.6 Subsonic Airfoil Aerodynamics

Using **PANEL** we now have a means of easily examining the pressure distributions, and forces and moments, for different airfoil shapes. In this section we present a discussion of airfoil characteristics using an inviscid analysis. All the illustrative examples were computed using program **PANEL**. We illustrate key areas to examine when studying airfoil pressure distributions using the NACA 0012 airfoil at 4° angle of attack as typical in Fig. 4-25.
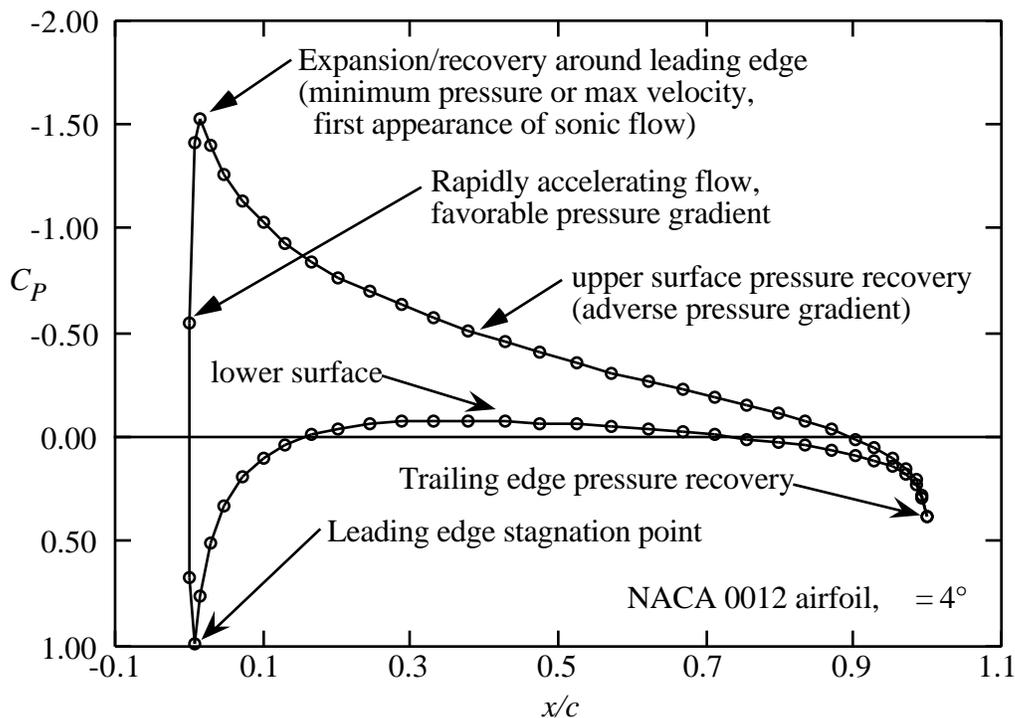
Figure 4-25. Key areas of interest when examining airfoil pressure distributions.

Remember that we are making an incompressible, inviscid analysis when we are using program **PANEL**. Thus, in this section we examine the basic characteristics of airfoils from that point of view. We will examine viscous and compressibility effects in subsequent chapters, when we have the tools to conduct numerical experiments. However, the best way to understand airfoil characteristics from an engineering standpoint is to examine the inviscid properties, and then consider changes in properties due to the effects of viscosity. Controlling the pressure distribution through selection of the geometry, the aerodynamicist controls, or suppresses, adverse viscous effects. The mental concept of the flow best starts as a flowfield driven by the pressure distribution that would exist if there were no viscous effects. The airfoil characteristics then change by the

"relieving" effects of viscosity, where flow separation or boundary layer thickening reduces the degree of pressure recovery which would occur otherwise. For efficient airfoils the viscous effects should be small at normal operating conditions.

4.6.1 Overview of Airfoil Characteristics: Good and Bad

In this section we illustrate the connection between the airfoil geometry and the airfoil pressure distribution. We identify and discuss ways to control the inviscid pressure distribution by changing the airfoil geometry. An aerodynamicist controls viscous effects by controlling the pressure distribution. Further discussion and examples providing insight into aerodynamic design are available in the excellent recent book by Jones.[13] A terrific book that captures much of the experience of the original designers of the NACA airfoils was written by aeronautical pioneer E.P. Warner.[14]

Drag: We discussed the requirement that drag should be zero[*] for this *two-dimensional* inviscid incompressible irrotational prediction method when we studied the accuracy of the method in the previous section. At this point we infer possible drag and adverse viscous effects by examining the effects of airfoil geometry and angle of attack on the pressure distribution.

Lift: Thin airfoil theory predicts that the lift curve slope should be 2π, and thick airfoil theory says that it should be slightly greater than 2π, with 2π being the limit for zero thickness. You can easily determine how close program **PANEL** comes to this value. These tests should give you confidence that the code is operating correctly. The other key parameter is a_{ZL}, the angle at which the airfoil produces zero lift (a related value is C_{L0}, the value of C_L at $\alpha = 0$).

Moment: Thin airfoil theory predicts that subsonic airfoils have their aerodynamic centers at the quarter chord for attached flow. The value of C_{m0} depends on the camber. We have seen in Fig. 4-21 that the computed aerodynamic center is not precisely located at the quarter chord. However, the slope of the moment curve in Fig. 4-21 corresponds to an aerodynamic center location of $x/c = 0.2597$, which is reasonably close to 0.2500.

Multi-element airfoils are also an important class of airfoils. However, their performance is so closely connect to the effects of viscosity that the discussion of those airfoils is deferred until Chapter 10, Viscous Flows in Aerodynamics.

---

[*] Three-dimensional panel methods can estimate the induced drag.
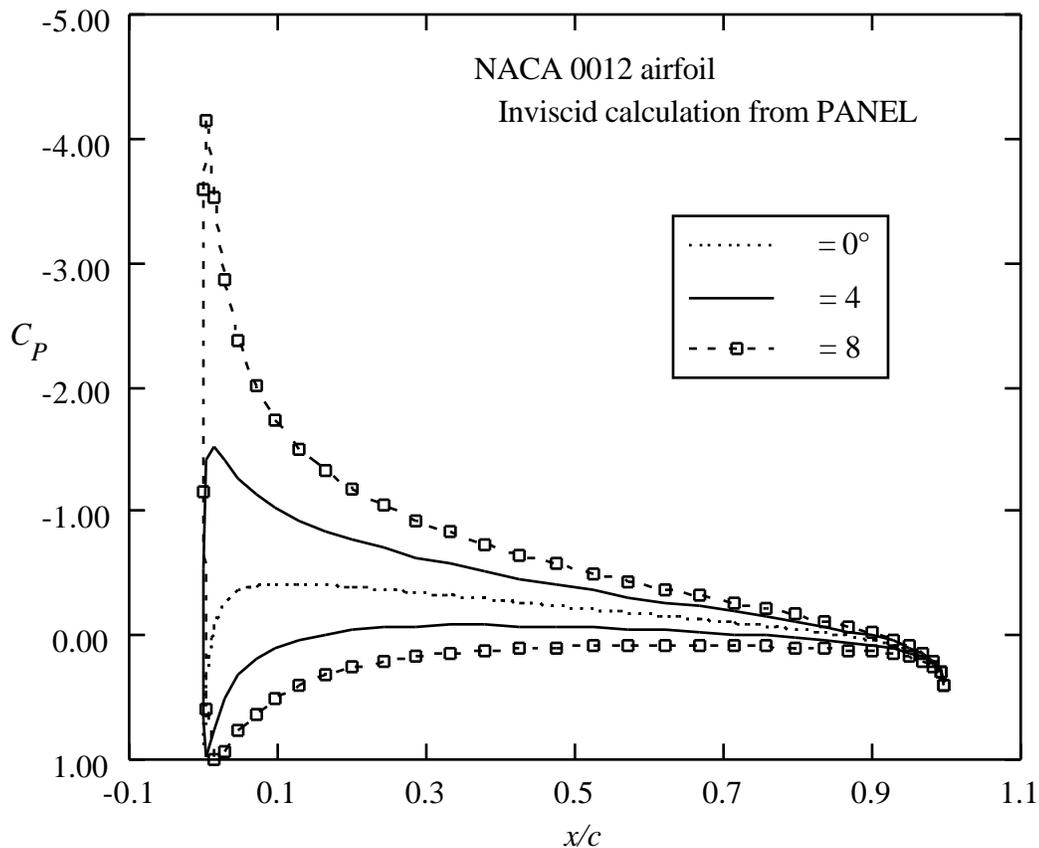
Figure 4-26. Effect of angle of attack on the pressure distribution.

The starting place for understanding airfoil characteristics is an examination of the angle of attack effects on an uncambered airfoil. Figure 4-26 presents this effect for the NACA 0012 airfoil. Here we see the progression from the symmetric zero angle of attack result. The $\alpha = 0°$ case produces a mild expansion around the leading edge followed by a monotonic recovery to the trailing edge pressure. As the angle of attack increases the pressure begins to expand rapidly around the leading edge, reaching a very low pressure, and resulting in an increasingly steep pressure recovery at the leading edge.

The next effect of interest is thickness. Figure 4-27 presents airfoil shapes for NACA 4 digit sections of 6, 12, and 18 percent thick. The associated basic pressure distributions at zero angle of attack are shown in Fig. 4-28. Clearly the thicker airfoil produces a larger disturbance, and hence a lower minimum pressure. However, the 18 percent thick airfoil produces a milder expansion around the leading edge and a recompression extending further upstream than the thinner airfoils, especially at the trailing edge.
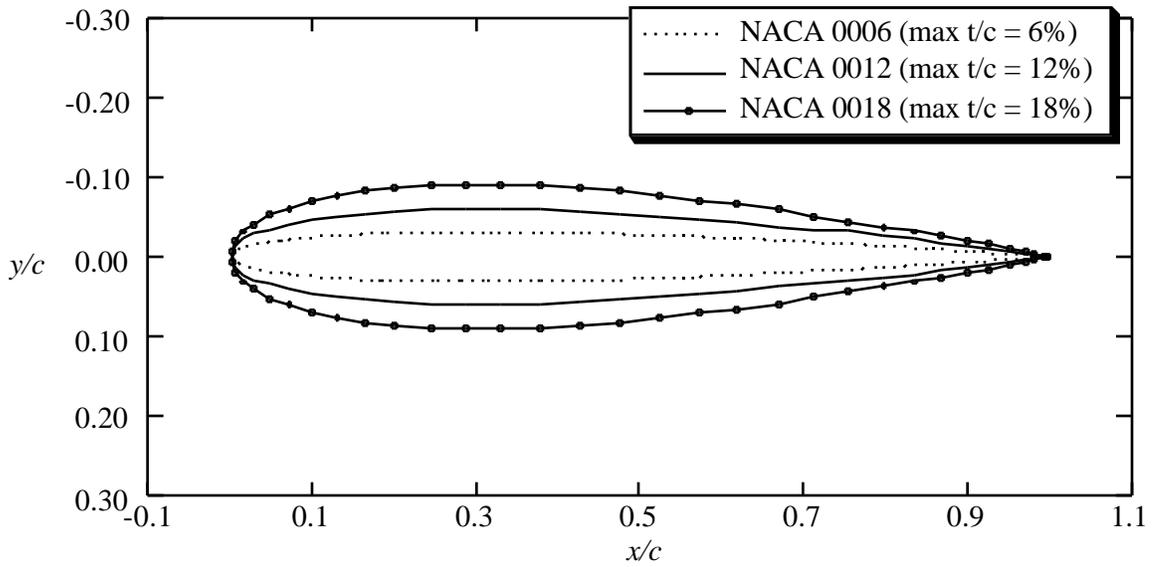
Figure 4-27. Comparison of NACA 4-digit airfoils of 6, 12, and 18% thicknesses.
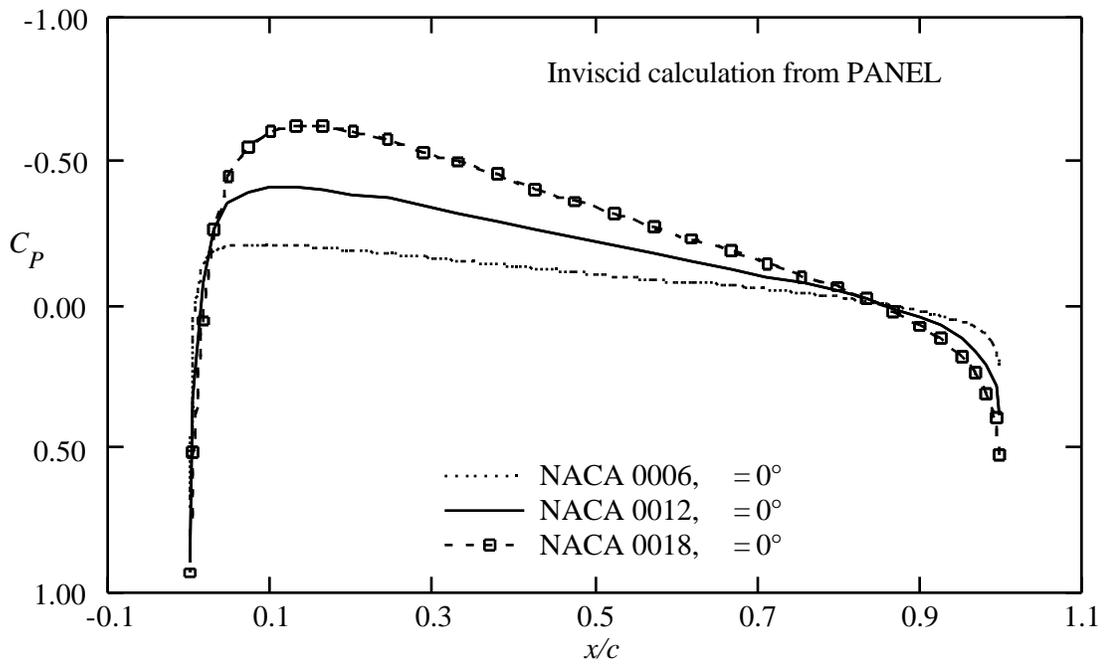
Figure 4-28. Effect of airfoil thickness on the pressure distribution at zero lift.

The effect of thickness in softening the expansion and recompression around the leading edge is even more evident at an angle of attack. Figure 4-29 shows this effect at a lift coefficient of .48. The thinnest airfoil shows a dramatic expansion/recompression due to the location of the stagnation point below the leading edge point, requiring a large expansion around the leading edge which has a very small radius of curvature. The thicker airfoil results in a significantly milder expansion and subsequent recompresion.
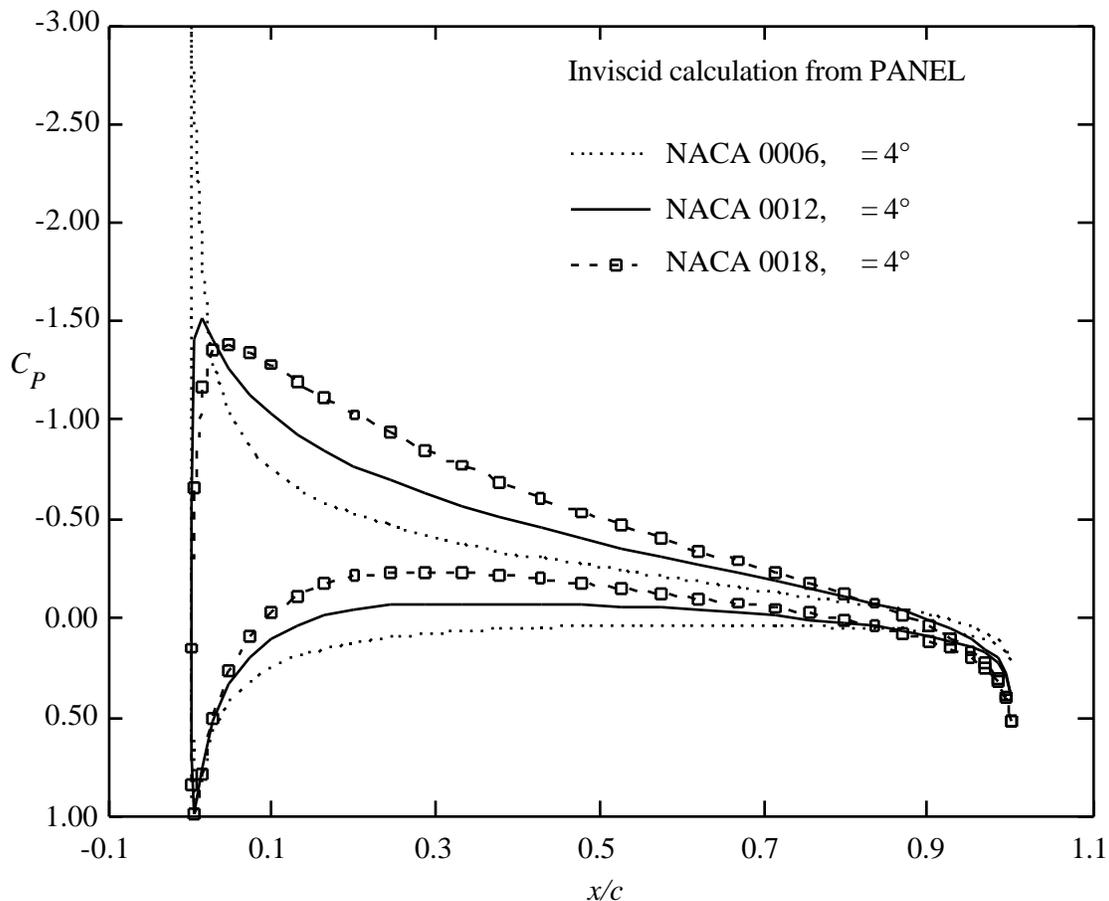
Figure 4-29. Effect of airfoil thickness on the pressure distribution at $C_L = 0.48$.

The next effect to examine is camber. Figure 4-30 compares the shapes of the NACA 0012 and 4412 airfoils. The pressure distributions on the cambered airfoil for two different angles of attack are shown in Figure 4-31. Note the role of camber in obtaining lift without producing a leading edge expansion followed by a rapid recompression immediately behind the expansion. This reduces the possibility of leading edge separation.
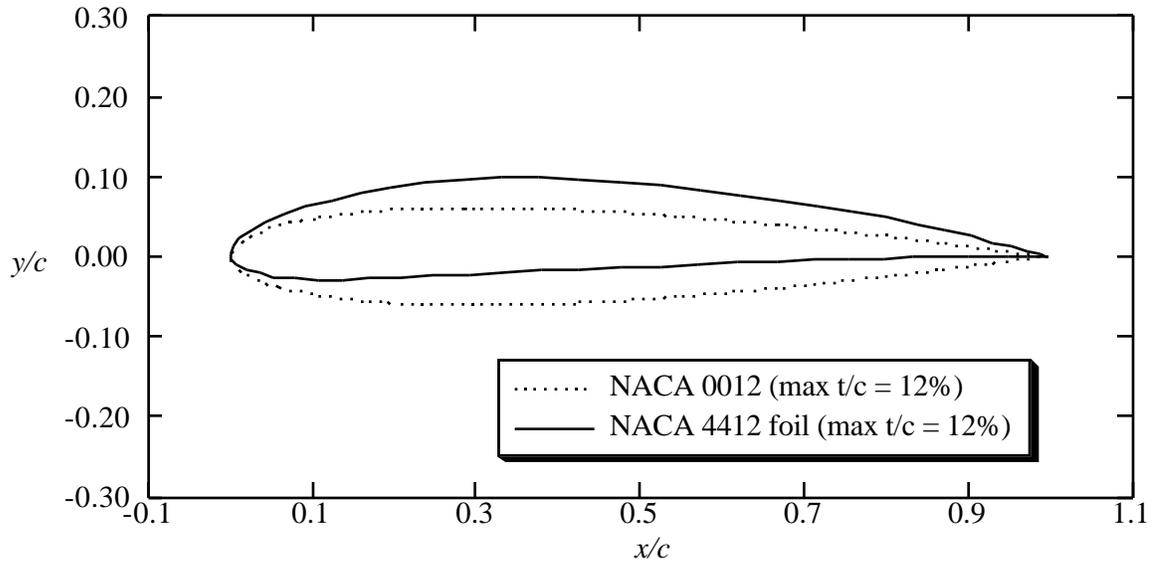
Figure 4-30. Comparison of uncambered and cambered NACA 4-digit airfoils.
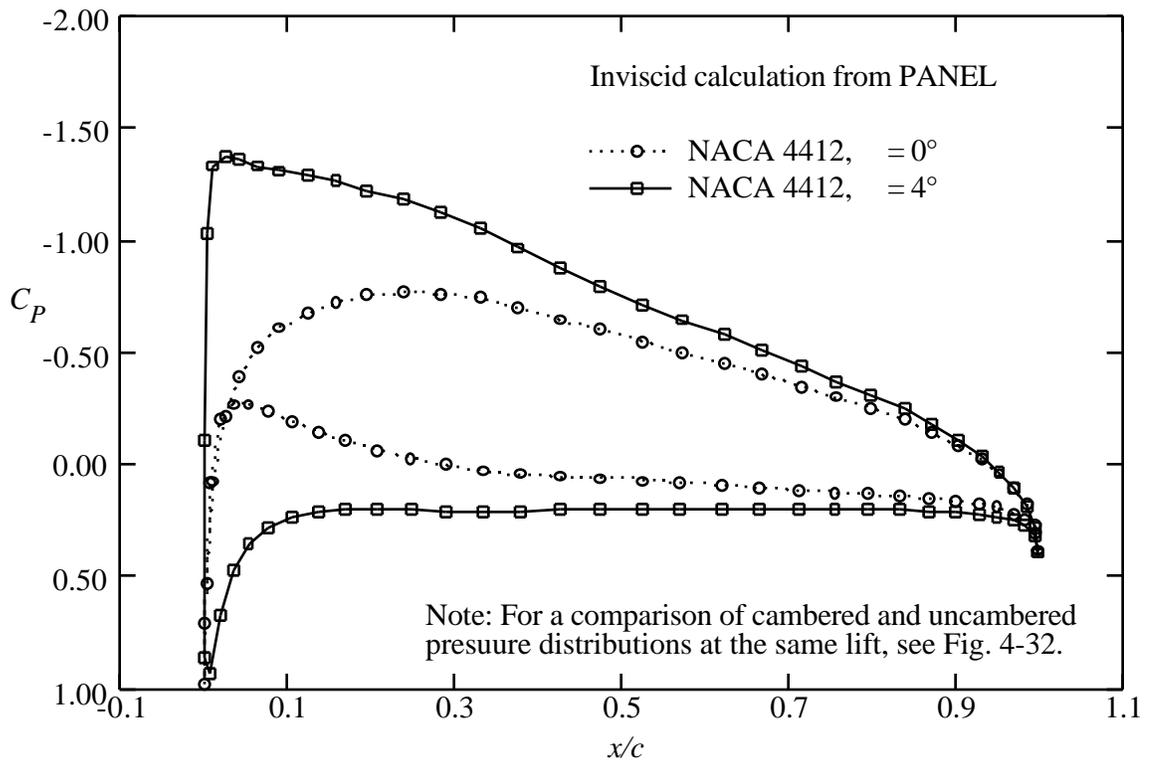
Figure 4-31. Effect of angle of attack on cambered airfoil pressure distributions at low lift.

A comparison of the NACA 0012 and NACA 4412 airfoil pressure distributions at the same lift coefficient is presented for several values of lift in Figures 4-32, 4-33 and 4-34. As the lift increases, the camber effects start to be dominated by the angle of attack effects, and the dramatic effects of camber are diminished until at a lift coefficient of 1.43 the pressure distributions start to look similar.
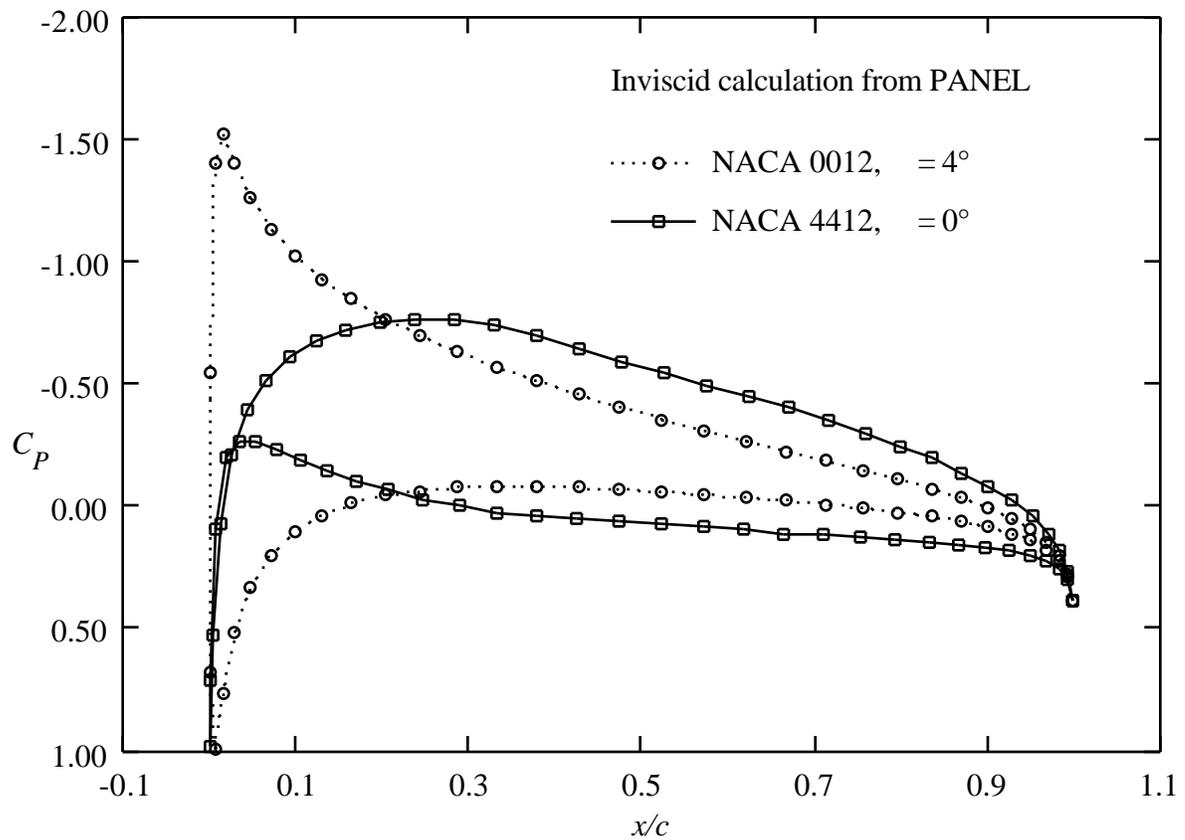
Figure 4-32. Camber effects on airfoil pressure distributions at C_L = 0.48.
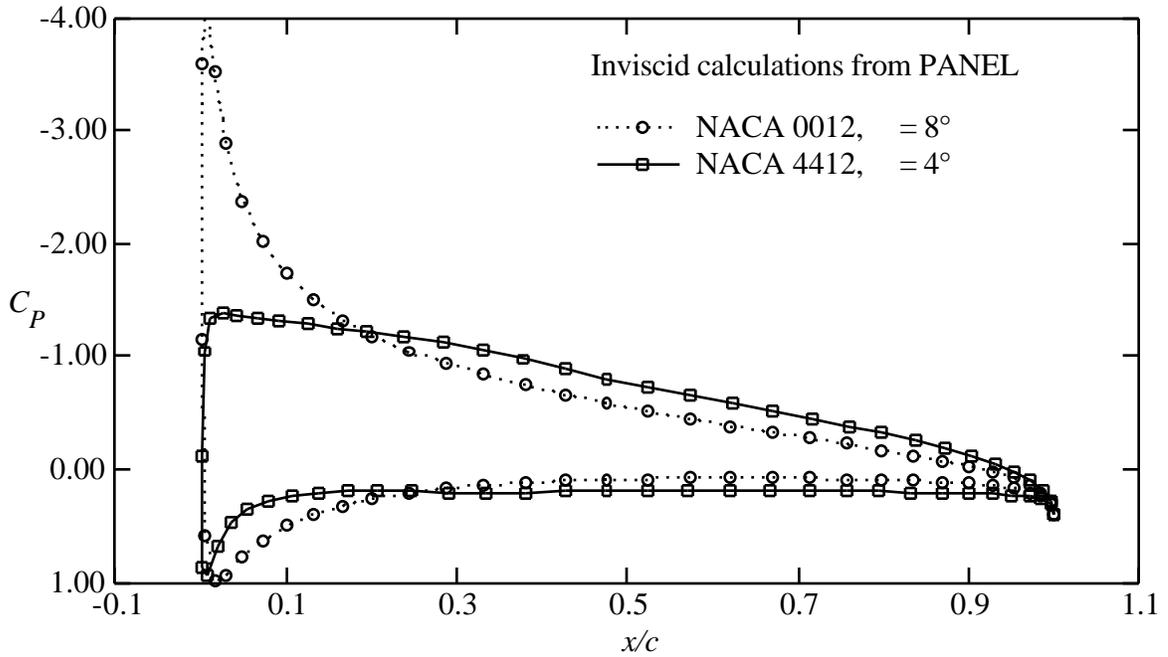
Figure 4-33. Camber effects airfoil pressure distributions at $C_L = 0.96$.
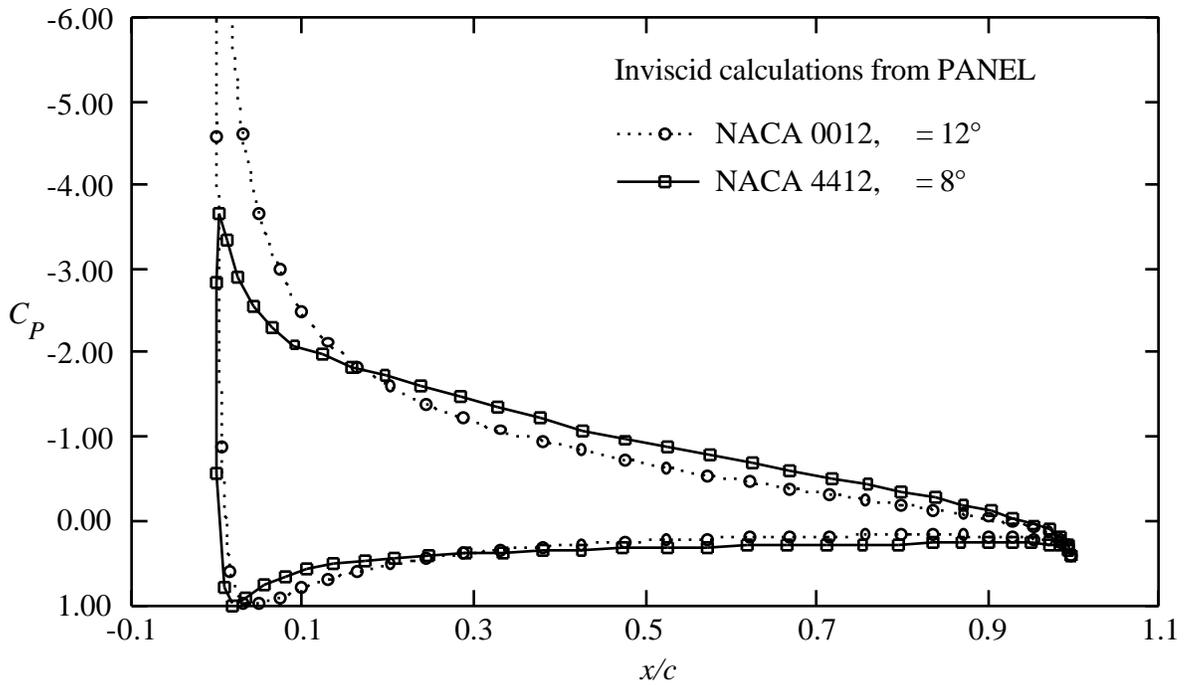
Figure 4-34. Camber effects airfoil pressure distributions at $C_L = 1.43$.

Finally, we examine the effect of extreme aft camber, which was part of the design strategy of Whitcomb when the so-called NASA supercritical airfoils were developed. This effect can be simulated using the NACA 6712 airfoil, as shown in Figure 4-35. The resulting pressure distribution is given in Figure 4-36. Note that the aft camber "opens up" the pressure distribution near the trailing edge. Two adverse properties of this type of pressure distribution are the large zero lift pitching moment and the delayed and then rapid pressure recovery on the upper surface. This type of pressure recovery is a very poor way to try to achieve a significant pressure recovery because the boundary layer will separate early. Whitcomb's design work primarily improved the pressure recovery curve.
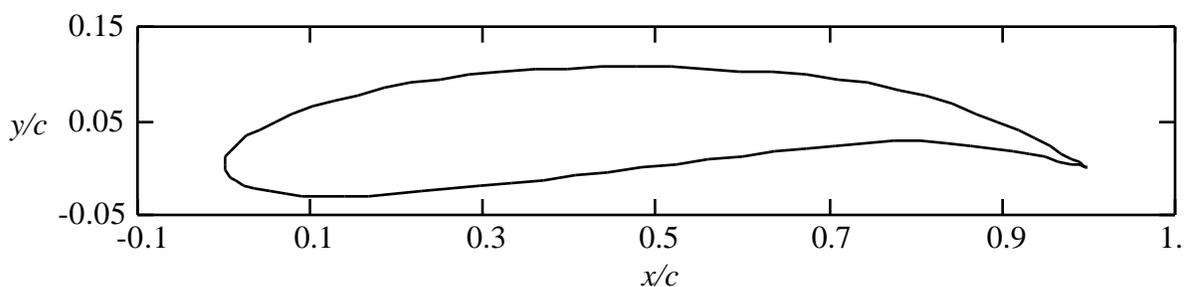
Figure 4-35. Highly aft cambered NACA airfoil, an NACA 6712.
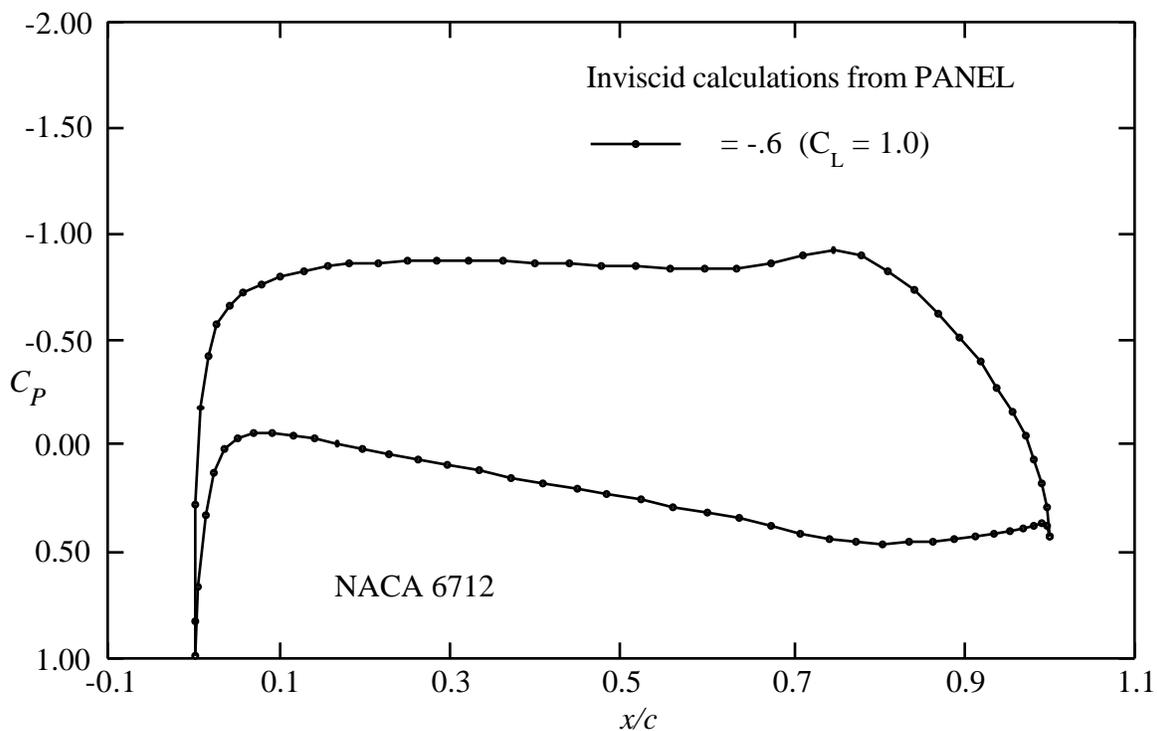
Figure 4-36. Example of the use of aft camber to "open up"
the pressure distribution near the trailing edge.

The airfoils used to demonstrate geometry effects on pressure distributions above use parametric geometry definition formulas developed in the 1930s. More modern airfoils are available to the aerodynamicist. Unfortunately, to obtain improved performance, the designs were developed without the use of simple geometric definitions, and are available only as tables of coordinates. One modern airfoil that extends some of the previous shapes to obtain a high performance airfoil is the GA(W)-1 airfoil.[15] This 17% thick airfoil designed by NASA's Richard Whitcomb provides better maximum lift and stall characteristics. Figure 4-37 shows the airfoil shape, and Fig. 4-38 shows the pressure distribution.
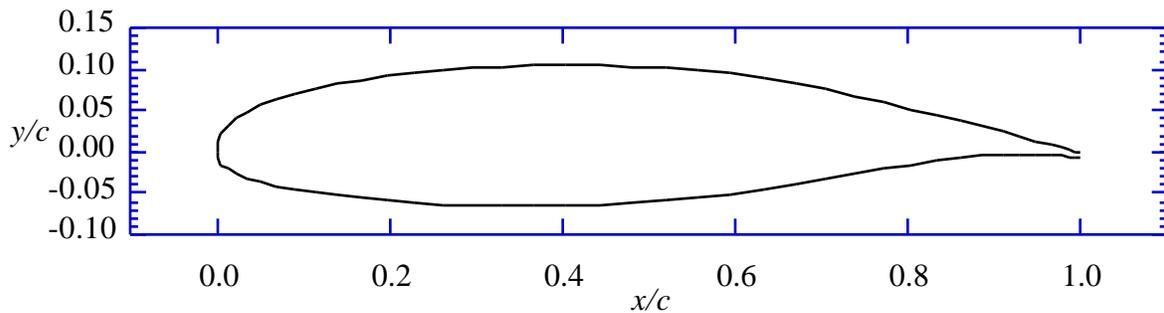
Figure 4-37. GA(W)-1 airfoil, also known as NASA LS(1)-0417.
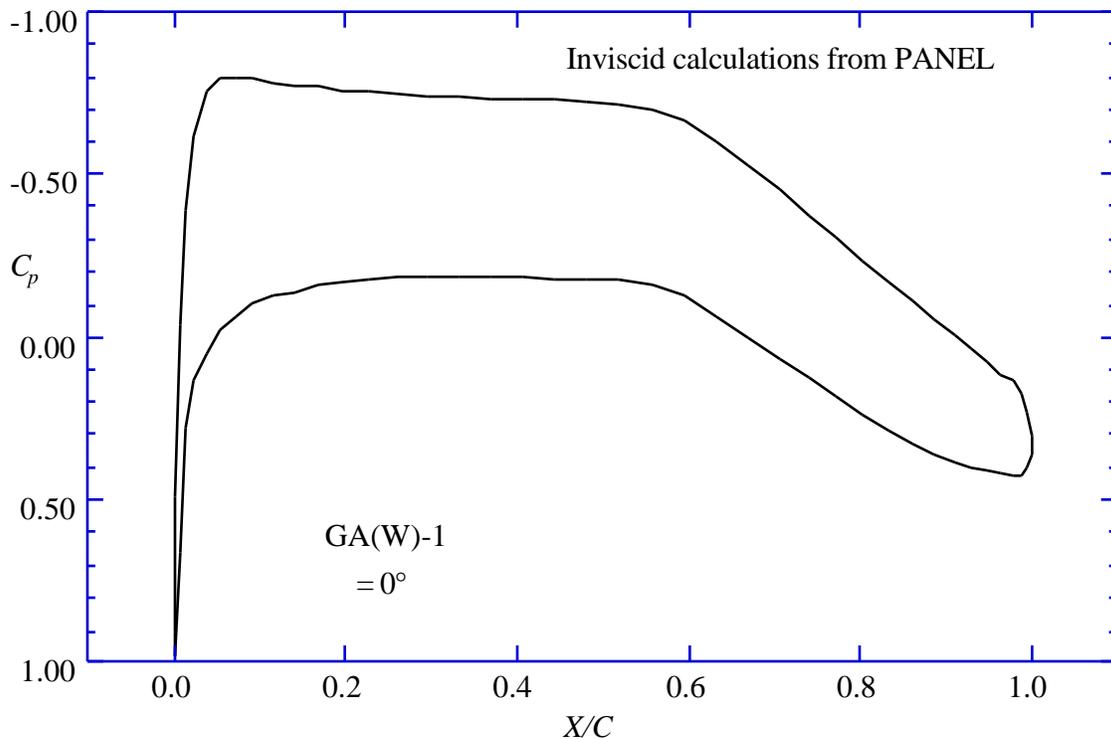
Figure 4-38. Pressure distribution at zero angle of attack of the GA(W)-1.

Notice that in this case the upper surface pressure distribution reaches a constant pressure plateau, and then has a moderate pressure recovery. Aft camber is used to obtain lift on the lower surface and "open up" the airfoil pressure distribution near the trailing edge in a manner suggested previously in Fig. 4-36. The area of aft camber on the lower surface is know as the "cove" region. If the camber is too extreme here the adverse pressure gradient will be too steep, and the flow will separate on the lower surface before it separates on the upper surface. Also, this type of pressure distribution has a significantly higher C_{m0} than conventional airfoil sections.

4.6.2 Geometry and Design

Effects of Shape Changes on Pressure Distributions: So far the examples have demonstrated global effects of camber and thickness. To develop an understanding of the typical effects of adding local modifications to the airfoil surface, Exercise 5 provides a framework for the reader to carry out an investigation analogous to the one for which results were presented in Section 4.6.1. It is also worthwhile to investigate the very powerful effects that small deflections of the trailing edge can produce. This reveals the power of the Kutta condition, and alerts the aerodynamicist to the basis for the importance of viscous effects at the trailing edge.

This approach is extremely educational when implemented in an interactive computer program, where the aerodynamicist can make shape changes with a mouse and see the effect on the pressure distribution immediately. An outstanding code that does this has been created by Ilan Kroo.[16] It is called **PANDA**, originally was for the Macintosh, but now is available for a PC.

Shape for a specified pressure distribution: There is another way that aerodynamicists view the design problem. The local modification approach described above is useful to make minor changes in airfoil pressure distributions. Often the aerodynamic designer wants to find the geometric shape corresponding to a prescribed pressure distribution from scratch. This problem is known as the inverse problem. This problem is more difficult than the analysis problem. It is possible to prescribe a pressure distribution for which no geometry exists. Even if the geometry exists, it may not be acceptable from a structural standpoint. For two-dimensional incompressible flow it is possible to obtain conditions on the surface velocity distribution that ensure that a closed airfoil shape exists. Excellent discussions of this problem have been given by Volpe[17] and Sloof.[18] A two-dimensional panel method has been developed by Bristow.[19] Numerical optimization can also be used to find the shape corresponding to a prescribed pressure distribution.[20]

4.7 Issues in the Problem formulation for 3D flow over aircraft

The extension of panel methods to three dimensions leads to fundamental questions regarding the proper specification of the potential flow problem for flow over an aircraft. Examples include the proper treatment of wing tips and the treatment of the wake and fuselage aft of the wing. Hess[21] provides an excellent discussion of the problems. In particular, the Kutta condition has to be reconsidered in three-dimensional flow. There are several aspects to consider. When solving the flow over a complete aircraft the aerodynamicist has to decide how to model the flow streaming off the fuselage or tip tank. The Kutta condition applies to distinct edges, and the inviscid model is not as precise. Many different approaches have been followed. Carmichael and Erickson[22] also provide good insight into the requirements for a proper panel method formulation. Similarly, references 4 and 5 provide good overviews.

Aerodynamics panel methods generally use quadrilateral panels to define the surface. Since three points determine a plane, the quadrilateral may not necessarily define a consistent flat surface. In practice, the methods actually divide panels into triangular elements to determine an estimate of the outward normal. It is important that edges fit so that there is no leakage in the panel model representation of the surface.

Other practical considerations also require fastidious attention to detail. These include making sure that the outward surface normal is oriented in the proper direction, that all surfaces are properly enclosed, and that wakes are properly specified. In some methods wakes are handled automatically. In other methods the wakes must be precisely specified by the user. This provides complete control over the simulation, but means that the user must understand precisely what the problem statement should be. Figure 4-39 shows an example of a panel model including the details of the wakes. For high lift cases and wakes from one surface streaming near another, wake deflection must be computed as part of the solution. Figure 4-39 comes from a one week "short" course that was given to prospective users of an advanced panel method known as PAN AIR.[23] Clearly, to ensure that the problem is properly specified, and to examine the entire flowfield in detail, a complete graphics capability is required.

There is one other significant difference. Induced drag occurs even in inviscid, irrotational incompressible flow. However, its calculation by integration of pressures over the surface requires extreme accuracy, as we saw above for the two-dimension examples. The use of a farfield momentum approach is much more accurate, and is described in Chap. 5, Drag, An Introduction.

Impermeable Surface

Tail Wake
Nor Shown

Body Wake

Carry-Over
Wakes
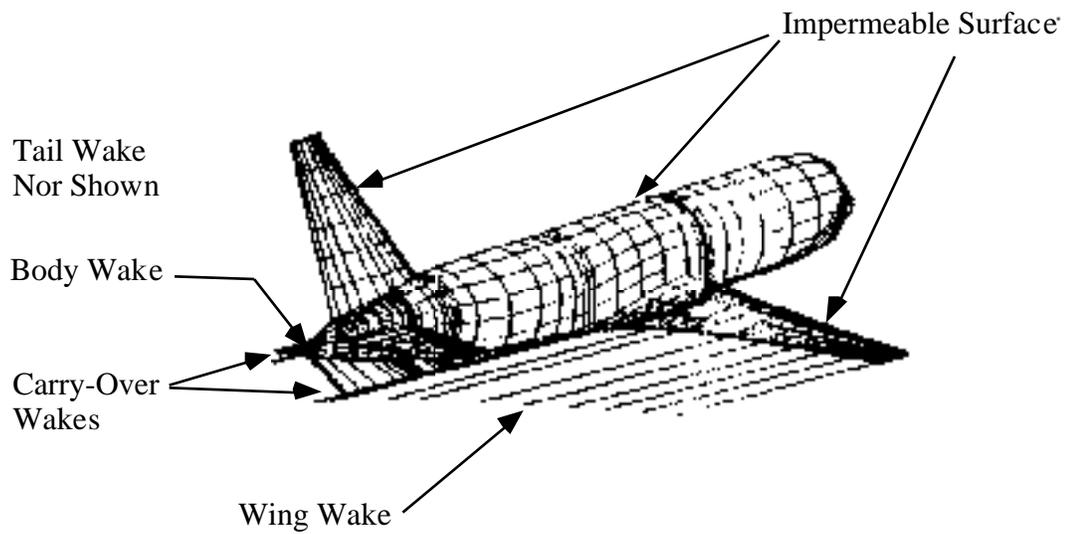
Wing Wake

a) wing-body-tail configuration panel scheme with wakes

Impermeable
Surfaces

Body Wake

Tail-Body
Carry-Over
Wake

Tail Wake

Wing-Body
Carry-Over
Wake
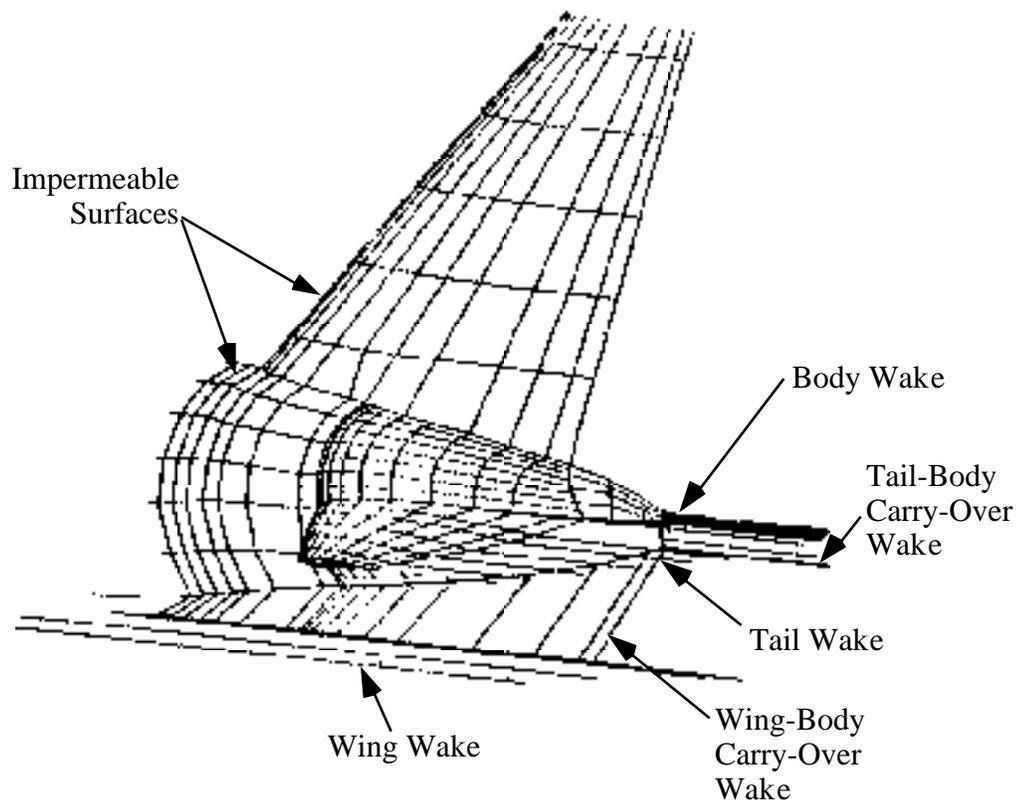
Wing Wake

b) details of the wake model required

Figure 4-39. Example of a panel model containing wake model details.
(from a viewgraph presented at a PAN AIR user's short course, Ref. 23)

4.8 Example applications of panel methods

Many examples of panel methods have been presented. Figure 4-40 shows an example of the use of a panel model to evaluate the effect of the space shuttle on the Boeing 747. This is a classic example. Other uses include the simulation of wind tunnel walls, support interference, and ground effects. Panel methods are also used in ocean engineering. Recent America's Cup designs have been dependent on panel methods for hull and keel design. The effects of the free surface can be treated using panel methods.
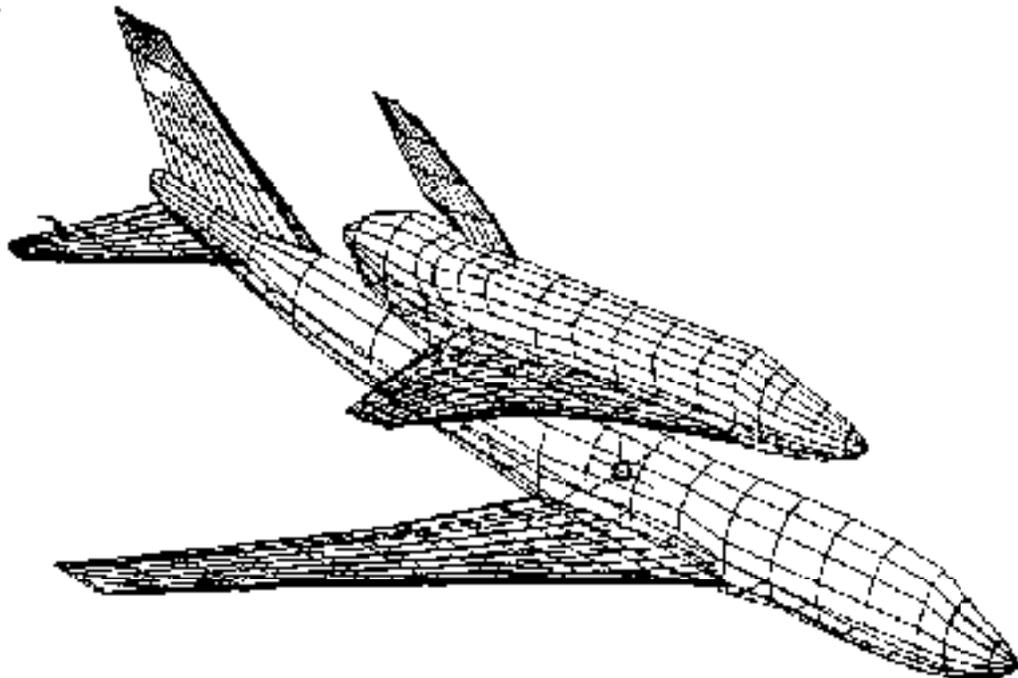
Figure 4-40. The space shuttle mounted on a Boeing 747.

One example has been selected to present in some detail. It is an excellent illustration of how a panel method is used in design, and provides a realistic example of the typical agreement that can be expected between a panel method and experimental data in a demanding real application. The work was done by Ed Tinoco and co-workers at Boeing.[24] Figure 4-41 shows the modifications required to modify a Boeing 737-200 to the 737-300 configuration.The panel method was used to investigate the design of a new high lift system. They used PAN AIR, which is a Boeing developed advanced panel method.[25]25 Figure 4-42 shows the panel method representation of the airplane.

Figure 4-41. The Boeing 737-300 relative to the model 737-200 (Ref.24).
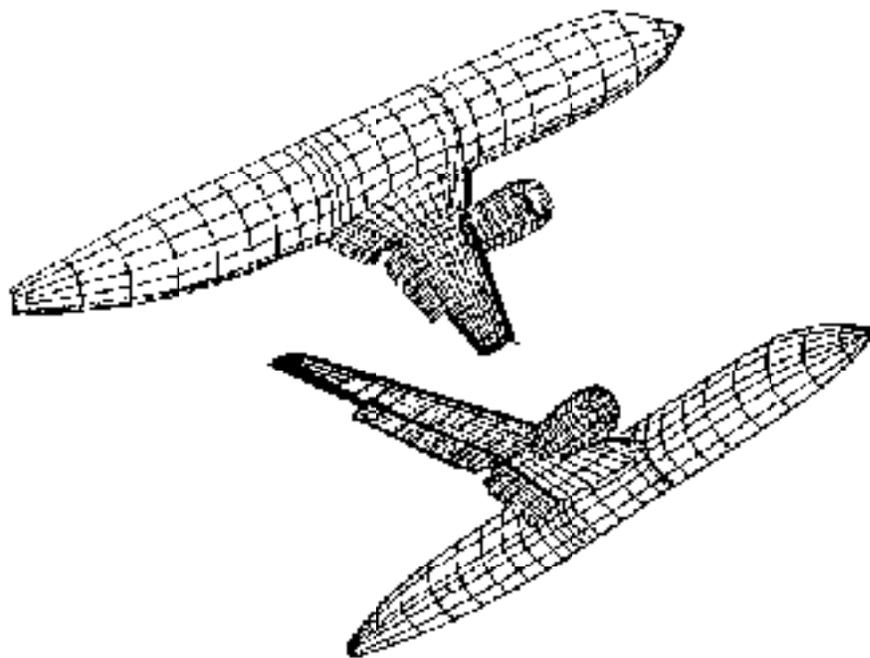
Figure 4-42. The panel representation of the 737-300 with 15° flap deflection (Ref. 4).

An understanding of the wing flowfield for two different takeoff flap settings was desired. The cases are "flaps 15", the normal takeoff setting, and "flaps 1", the high altitude, hot day setting. The work was conducted in concert with the flight test program to provide insight into the flight test results by providing complete flowfield details not available from the flight test. The computational models used 1750 panels for flaps 1 and 2900 panels for flaps 15. The modeling used to simulate this flowfield illustrates typical idealizations employed when applying panels methods to actual aircraft. Although typical, it is one of the most geometrically complicated examples ever published.

Figure 4-43 shows the wing leading edge and nacelle. The inboard Krueger flap was actually modeled as a doublet of zero thickness. The position was adjusted slightly to allow the doublet sheet to provide a simple matching of the trailing edge of the Krueger and the leading edge of the wing. These types of slight adjustments to keep panel schemes relatively simple are commonly used. The outboard leading and trailing edge flap geometries were also modified for use in this inviscid simulation. Figure 4-44 a) shows the actual and computational flaps 1 geometry. In this case the airfoil was modeled as a single element airfoil. The flaps 15 trailing edge comparison between the actual and computational geometry is shown in Fig. 4-44 b). The triple slotted flap was modeled as a single element flap. At this setting the gap between the forward vane and main flap is closed, and the gap between the main and aft flap is very small.

Figure 4-43. Inboard wing leading edge and nacelle details (Ref. 24).

a) Comparison of actual and computational wing geometry for the flaps 1 case (Ref. 24).

Actual Geometry

Computational Geometry
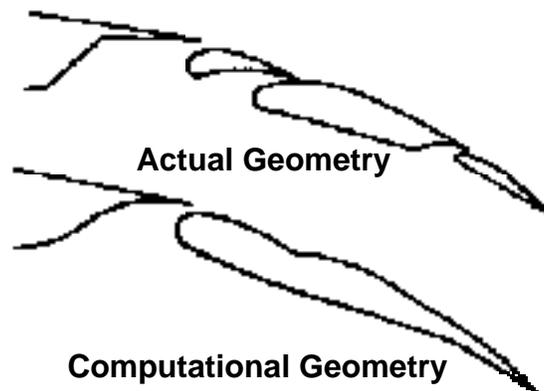
b) Actual and computational trailing edge geometry for the flaps 15 case (Ref. 4).

Figure 4-44. Examples of computational modeling for a real application.

Several three-dimensional modeling considerations also required attention. In the flaps 1 case shown in Fig. 4-45, spanwise discontinuities included the end of the outboard leading edge slat and trailing edge discontinuities at the back of the nacelle installation (called the thrust gate) between the inboard and outboard flaps. At the outboard leading edge the edges of the slat and wing were paneled to prevent leakage. A 0.1 inch gap was left between these surfaces. At the trailing edge discontinuity a wake was included to model a continuous trailing edge from which a trailing vortex sheet could be shed.

Figure 4-45. Spanwise discontinuity details requiring modeling for flaps 1 case (Ref. 24).

Similar considerations are required for the flaps 15. Here, special care was taken to make sure that the configuration was closed, and contained no holes in the surface at the ends of the flap segments.

Another consideration is the nacelle model. This requires the specification of the inlet flow at the engine face, a model of the strut wake, and both the outer bypass air plume and the primary wake from the inner hot gas jet. Figure 4-46 provides the details.

Figure 4-46 Nacelle model (Ref. 24).

Complete details of the model are contained in Ref. 24. With the model complete, the solution was obtained. The spanwise distribution of airfoil section lift coefficients is presented in Figure 4-47. The first part of the figure shows the results for the flaps 1 case, and the second part of the figure presents the flaps 15 case. In both cases the jig shape and flight shape including aeroelastic deformation are included. This is another consideration in making a proper aerodynamic simulation. In both cases the shape including the deformation under load shows much better agreement with flight and wind tunnel data. Notice the loss of lift on the wing at the nacelle station, and the decrease in lift outboard of the trailing edge flap location.

a) flaps 1 case

b) flaps 15 case

Figure 4-47. Spanwise distribution of lift coefficient on the Boeing 737-300 (Ref.24).

Figure 4-48 presents the change in section lift coefficient with angle of attack at several span stations. The agreement between PAN AIR and flight test is better for the flaps 1 case. Viscous effects are becoming important for the flaps 15 case.

a) flaps 1 case

b) flaps 15 case

Figure 4-48. Comparison of section lift coefficient change with angle of attack(Ref.24)

Figure 4-49 completes this example by presenting the comparison of pressure distributions for the two cases at four spanwise stations. The flaps 1 case agreement is generally good. Calculations are presented for both the actual angle of attack, and the angle of attack which matches the lift coefficient. Matching lift coefficient instead of angle of attack is a common practice in computational aerodynamics. Considering the simplifications made to the geometry and the absence of the simulation of viscous effects the agreement is very good. The flaps 15 case starts to show the problems that arise from these simplifications. This is a good example of the use of a panel method. It illustrates almost all of the considerations that must be addressed in actual applications.

a) flaps 1 case   b) flaps 15 case

Figure 4-49. Comparison of pressure distributions between flight and computations for the 737-300, solid line is PAN AIR at flight lift, dashed line is PAN AIR at flight angle of attack (Ref. 24).

4.9 Using Panel Methods

4.9.1 Common sense rules for panels

- Vary the size of panels smoothy
- Concentrate panels where the flowfield and/or geometry is changing rapidly
- Don't spend more money and time (i.e., numbers of panels) than required

Panel placement and variation of panel size affect the quality of the solution. However, extreme sensitivity of the solution to the panel layout is an indication of an improperly posed problem. If this happens, the user should investigate the problem thoroughly.

Panel methods are an aid to the aerodynamicist. You must use the results as a guide to help you develop your own judgement. (An issue: lawyers often get involved because you frequently sign an agreement that the code developer is not liable for problems that stem from the use of the code; the same disclaimer you see with every PC programs).

Remember that the panel method solution is an approximation of the real life problem; an idealized representation of the flowfield. An understanding of aerodynamics that provides an intuitive expectation of the types of results that may be obtained, and an appreciation of how to relate your idealization to the real flow is required to get the most from the methods. This insight requires experience and study.

4.9.2 What a Panel Method Can't Do

1. Panel methods are inviscid solutions. You will not capture viscous effects except via user "modeling" by changing the geometry.

2. Solutions are invalid as soon as the flow develops local supersonic zones [i.e., $C_p < C_{pcrit}$]. For two-dimensional isentropic flow, the exact value of C_p for critical flow is:

$$C_{pcrit} = -\frac{2}{M^2}\left[1 - \left[\frac{1 + \frac{-1}{2}M^2}{\frac{+1}{2}}\right]^{\overline{-1}}\right] \qquad (4\text{-}96)$$

4.10 Advanced panel methods: What is a "Higher Order" Panel Method?

So-called "higher-order" panel methods use singularity distributions that are not constant on the panel, and may also use panels which are non-planar. Higher order methods were found to be crucial in obtaining accurate solutions for the Prandtl-Glauert Equation at supersonic speeds. At supersonic speeds, the Prandtl-Glauert equation is actually a wave equation (hyperbolic), and

2/24/98

requires much more accurate numerical solution than the subsonic case in order to avoid pronounced errors in the solution (Magnus and Epton[25]). However, subsonic higher order panel methods, although not as important as the supersonic flow case, have been studied in some detail. In theory, good results can be obtained using far fewer panels with higher order methods. In practice the need to resolve geometric details often leads to the need to use small panels anyway, and all the advantages of higher order panelling are not necessarily obtained. Nevertheless, since a higher order panel method may also be a new program taking advantage of many years of experience, the higher order code may still be a good candidate for use.

4.11 Today's standard programs: a brief survey

Panel methods are widely used in the aircraft industry, and have been for a long time. Comparisons between codes have been made, the most recent comparison being by Margason, et al.[26] In general, all the new professionally-developed codes work well. The selection of a specific code will likely be based on non-technical considerations. In recent times, several codes have emerged as the primary ones. The newest is known as PMARC,[27] for Panel Method Ames Research Center. These codes have received the most development effort. We provide a brief description of the codes a new aerodynamicist will most likely encounter. Specific references are provided in Tables 4-1 through 4-3.

PAN AIR - Boeing-developed code, funded by a variety of government agencies, and available through COSMIC (a lease arrangement, about $7000 last time I looked, and export controlled).

This code provides total flexibility, i.e., it's really an integral equation solver and not an aerodynamicist's tool *per se*. It uses higher order panels, and is both subsonic and supersonic. It's relatively expensive and difficult to run (a PAN AIR user would take months to train, and it would probably become his primary job).

To effectively use the code good pre- and post- processing systems must be available. Although Boeing has these systems in place, they were internally developed and are not available outside the company.

VSAERO - AMI developed (Analytical Mechanics Inc., Frank Dvorak and Brian Maskew). It uses low order panels and is subsonic only. It also handles general geometries, and includes options to treat viscous effects and vortex flows. The original NASA version is available through COSMIC. However, the code has been much further developed by AMI and is for sale by this company. The price for the current code is about $100K, and they also have a plotting package (OMNIPLOT, about $20K) available for purchase. This code also requires considerable user training. Support from AMI is about $10-$15K per year, and site licensing is not available (as of 1990). You pay a

large fee for each machine on which you install VSAERO. The business of licensing codes from developers is an important consideration in computational aerodynamics in the '90s.

The public domain version of this code was obtained by several groups that worked on the design of the America's Cup Yacht competitors in the mid-eighties. The code was used for hull and keel design. One of the modifications that was made was the addition of the free surface representing the air-water interface (recall that the free surface problem means that the surface displacement is unknown, and the boundary condition is that a constant pressure exists at the interface).

QUADPAN - Lockheed-developed, and possibly developed at some government labs. Not widely used by industry outside of Lockheed. This is probably because of availability.

Versions of the "Hess Code" - further developments of the team at Douglas now led by Hess. Naturally, Douglas uses this code exclusively. Douglas developed numerous versions under various government contracts, and it seems to be available mainly at Navy facilities.

Woodward: An old panel method that is sometimes encountered is the code known as the "Woodward" or "Woodward-Carmichael" code. Woodward was a pioneer panel method developer, and the most likely Woodward code a new aerodynamicist might encounter is a version of USSAERO, which was developed under NASA contract. Woodward's first methods were developed while he was at Boeing, and were supported by NASA Ames, primarily for the US SST program (which was an important national effort in the sixties). Subsequently, Woodward went into business and continued to develop codes. USSAERO treats both supersonic and subsonic flow, and a version which incorporates design options "Woodward 1-2" is available at VPI.

PMARC -This is the newest panel method code, and was developed at NASA Ames to provide an extremely flexible method to simulate a wide range of very general geometries. An example is the simulation of high lift systems and jet exhausts for VSTOL aircraft. The code is a lower order panel method, and can simulate steady as well as unsteady flow. The wake position can be obtained as part of the solution. It is being used for underwater applications as well as for aircraft. This code is also available at VPI.

The history of panel methods is illustrated in the tables. Table 4-1 summarizes some of the key early methods that were developed. W12SC3 is included because it was a valuable combination of two early codes, providing significant design capability, particularly at supersonic speeds. Table 4-2 reviews the extremely active era of the development of advanced methods. Finally, Table 4-3 provides details on the current production codes likely to be used on current aerodynamic design and analysis projects.

Table 4 - 1
Comparison of Some Major Panel Method Programs: Early Codes

Originator and Method Name	Year	Panel Geometry	Source Type	Doublet Type	Boundary Conditions	Restrictions	Comments
Hess and Smith[1] (Douglas)	1962	flat	constant	none	specification of normal flow	non-lifting wings and bodies only	
Rubbert[2] (vortex lattice)	1964	flat	none	constant	normal flow	planar wings only	
Woodward[3] (Woodward I)	1967	flat	constant	linear	normal flow	wings must be planar	mainly supersonic, includes design & optimization
Rubbert and Saaris[4] (Boeing A-230)	1968	flat	constant	constant	normal flow	nearly constant panel density	
Hess I[5]	1972	flat	constant	linear	normal flow	wings and bodies only	
USSAERO[6] (Woodward II)	1973	flat					subsonic and supersonic, analysis only
W12SC3[7] (Grumman)	1983	flat			mixed design and analysis		combines Woodward 1 & 2 features

1. Hess, J.L., and Smith, A.M.O., "Calculation of Nonlifting Potential Flow About Arbitrary Three-Dimensional Bodies," Douglas Report ES40622, Douglas Aircraft Company, 1962.

2. Rubbert, P.E., "Theoretical Characteristics of Arbitrary Wings by a Nonplanar Vortex Lattice Method," Boeing Report D6-9244, The Boeing Company, 1964.

3. Woodward, F.A., Tinoco, E.N., and Larsen, J.W., "Analysis and Design of Supersonic Wing-Body Combinations, Including Flow Properties in the Near Field," Part I - Theory and Application, NASA CR-73106, 1967.

4. Rubbert, P.E., and Saaris, G.R., "A General Three-Dimensional Potential Flow Method Applied to V/STOL Aerodynamics," SAE Paper No. 680304, 1968.

5. Hess, J.L., "Calculation of Potential Flow About Arbitrary 3-D Lifting Bodies," Douglas Report MDC-J5679-01, October 1972.

6. Woodward, F.A., "An Improved Method for the Aerodynamic Analysis of Wing-Body-Tail Configurations in Subsonic and Supersonic Flow," NASA CR-2228, Parts I and II, 1973.

7. Mason, W.H., and Rosen, B.S., "The COREL and W12SC3 Computer Programs for Supersonic Wing Design and Analysis," NASA CR 3676, 1983 (contributions by A. Cenko and J. Malone acknowledged).

from Magnus and Epton, NASA CR 3251, April 1980 (with extensions)

Table 4 - 2
Comparison of Some Major Panel Method Programs: Advanced Methods

Originator and Method Name	Year	Panel Geometry	Source Type	Doublet Type	Boundary Conditions	Restrictions	Comments
Roberts and Rundle[1]	1973	paraboloidal	quadratic	quadratic	normal flow		numerical integration, very expensive
Mercer, Weber and Lesford[2]	1973	flat	none	smooth, cubic/ quadratic	normal flow in least squares sense	planar wings	subsonic/ supersonic, cubic spanwise, quadratic chordwise
Morino and Kuo[3] (SOUSSA)	1974	continuous, hyperbo-loidal	constant	constant	potential	no thin configura-tions	unsteady
Johnson and Rubbert[4]	1975	paraboloidal	linear	quadratic	normal flow		
Ehlers and Rubbert[5] (Mach line paneling)	1976	flat	linear	continuous quadratic	normal flow	planar wings, special paneling	supersonic flow
Ehlers et al.[6] (PAN AIR "pilot code")	1977	continuous piecewise flat	linear	continuous quadratic	arbitrary in		subsonic and supersonic

[1] Roberts, A., and Rundle, K., "Computation of First Order Compressible Flow About Wing-Body Configurations," AERO MA No. 20, British Aircraft Corporation, February, 1973.

[2] Mercer, J.E., Weber, J.A., and Lesford, E.P., "Aerodynamic Influence Coefficient Method Using Singularity Splines," NASA CR-2423, May 1974.

[3] Morino, L., and Kuo, C-C, "Subsonic Potential Aerodynamics for Complex Configurations: A General Theory," *AIAA Journal*, Vol. 12, No. 2, pp 191-197, February, 1974.

[4] Johnson, F.T., and Rubbert, P.E., "Advanced Panel-Type Influence Coefficient Methods Applied to Subsonic Flow," AIAA Paper No. 75-50, January 1975.

[5] Ehlers, F.E., and Rubbert, P.E., "A Mach Line Panel Method for Computing the Linearized Supersonic Flow," NASA CR-152126, 1979.

[6] Ehlers, F.E., Epton, M.A., Johnson, F.T., Magnus, A.E., and Rubbert, P.E., "A Higher Order Panel Method for Linearized Flow," NASA CR-3062, 1979.

from Magnus and Epton, NASA CR 3251, April 1980 (with extensions)

Table 4-3
Comparison of Some Major Panel Method Programs: Production Codes

Originator and Method Name	Year	Panel Geometry	Source Type	Doublet Type	Boundary Conditions	Restrictions	Comments
MCAIR [1] (McDonnell)	1980	flat	constant	quadratic			design option
PAN AIR [2] (Boeing)	1980	continuous piecewise flat	continuous linear	continuous quadratic	arbitrary in ,		subsonic and supersonic
Hess II [3] (Douglas)	1981	parabolic	linear	quadratic	normal flow		
VSAERO[4] (AMI)	1981	flat	constant	constant	exterior and interior normal flow		subsonic
QUADPAN [5] (Lockheed)	1981	flat	constant	constant			
PMARC [6] (NASA Ames)	1988	flat	constant	constant			unsteady, wake rollup

[1] Bristow, D.R., "Development of Panel Methods for Subsonic Analysis and Design," NASA CR 3234, 1980.

[2] Magnus, A.E., and Epton, M.A., "PAN AIR - A Computer Program for Predicting Subsonic or Supersonic Linear Potential Flows About Arbitrary Configurations Using a Higher Order Panel Method," Volume I - Theory Document (Version 1.0), NASA CR 3251, 1980.

[3] Hess, J.L., and Friedman, D.M., "An Improved Higher Order Panel Method for Three Dimensional Lifting Flow," Douglas Aircraft Co. Report No. NADC-79277-60, 1981.

[4] Maskew, B., "Prediction of Subsonic Aerodynamic Characteristics: A Case for Lower Order Panel Methods," AIAA Paper No. 81-0252, 1981.

[5] Coopersmith, R.M., Youngren, H.H., and Bouchard, E.E., "Quadrilateral Element Panel Method (QUADPAN)," Lockheed-California LR 29671, 1981.

[6] Ashby, D.L., Dudley, M.R., and Iguchi, S.K., "Development and Validation of an Advanced Low-Order Panel Method," NASA TM 101024, 1988 (also TM 102851, 1990).

from Magnus and Epton, NASA CR 3251, April 1980 (with extensions)

4.12 Exercises

1. Program **PANEL**.

   a) Obtain a copy of program **PANEL** and the sample case.

   b) Convert **PANEL** to run on your PC.

   c) Run the sample case: NACA 4412, 20 pts. upper, 20 pts. lower, $= 4°$, and verify against sample case.

   d) Document
         i)   compile time required on your PC
                (cite computer and compiler used)
         ii)   the execution time for the sample case
         iii) the accuracy relative to the sample case.
         iv) the exact modifications required to make the code
                work on your computer

2. Start work on program **PANEL**

   a) Save a reference copy of the working code!

   b) Check convergence with panels (NLOWER+NUPPER must be less than 100 currently). How many panels do you need to get results independent of the number of panels? What happens to the computer time as the number of panels increases?

   c) Check the coordinates generated by the airfoil routine vs. exact (consider using the NACA 0012, see App. A for geometry definition), including examination of the coordinates at the trailing edge. This is best done by making a table of exact and computed values at selected values of x/c. What did you find out?

   d) Locate the source strengths, and sum the source strengths x panel lengths to get the total source strength. Does it sum to zero? Should it?

   e) Where is the moment reference center in this code?

   Submit an assessment of your findings.

3. Modify program **PANEL**:

   You need a version of **PANEL** that will allow you to compute the pressure distribution on arbitrary airfoils. This exercise will give you this capability. Modify the code to interpolate input airfoil points to the program defined surface points, x/c. The resulting code should:

   a) accept arbitrary airfoil input data

   b) echo all the input data on the output

   c) generate an output file for post processing

      (both for plotting and as the input to a boundary layer code)

   d) output Cm about the airfoil quarter chord point.

   Hint: Don't alter the panel distribution. The paneling scheme should be independent of the input distribution of airfoil coordinates. This produces a much more general and accurate program. This problem is usually solved by finding both the x/c and y/c

values as functions of the airfoil arc length, starting at the lower surface trailing edge. A spline fit is usually used to interpolate the values along the arc length.

Check your modified code. Run the airfoil you ran previously with internal coordinate generation. This time use an input file with the same coordinates as external inputs. Submit a description of your work, and assess your results.

4. Assess the accuracy of incompressible potential flow theory. Run your modified **PANEL** code using the airfoil you selected in the exercise in Chap. 1. (What happens if your airfoil has a trailing edge with finite thickness? What do you do now?)

- compare the computed pressure distribution with the experimental data
- compare the computed force and moment results with the data
  (over a range of angles of attack

Turn in a CONCISE report describing the results of your work. Include a plot showing the pressure distribution comparison, and a plot(s) showing comparison with forces and moments. What do you conclude about the accuracy of this method?

5. Airfoil design using program **PANEL**

Take your reference airfoil:

   a) add thickness on the bottom (mid chord)- what happens?
   b) shave some thickness off the bottom (mid chord) - ?
   c) add thickness on the top (mid chord)- what happens?
   d) deflect the trailing edge down a couple of degrees
      (how sensitive is the airfoil to changes at the TE?)

Hint: use smooth   's to the reference foil employing analytic formulas.

Turn in a CONCISE report comparing the effects on the pressure distribution due to the above modifications.

6. How good is thin airfoil theory? Compare the thin airfoil Cp for a flat plate with program **PANEL**.

Recall thin airfoil theory for an uncambered flat plate:

$$C_p = 4 \sqrt{\frac{(1 - x/c)}{x/c}} \; .$$

a) pick an NACA 0012 airfoil at $= 2°$ and $12°$ and run **PANEL**.
b) plot $Cp/$ as a function of x/c.
c) how many panels do you need to get a converged solution from **PANEL**?
d) what conclusions do you reach?

4.13 References

[1] Anderson, John P., Jr., *Modern Compressible Flow*, 2nd Ed., McGraw-Hill, New York, 1990, pp. 258-269.

[2] Hess, J. L., "Panel Methods in Computational Fluid Dynamics," *Annual Review of Fluid Mechanics*, Vol. 22, 1990, pp. 255-274.

[3] Hess, J.L., "Linear Potential Schemes," *Applied Computational Aerodynamics*, P.A. Henne, ed., AIAA, Washington, 1990. pp.21-36.

[4] Erickson, L.L., "Panel Methods—An Introduction," NASA TP-2995, Dec. 1990.

[5] Katz, J., and Plotkin, A., Low-Speed Aerodynamics From Wing Theory to Panel Methods, McGraw-Hill, Inc., New York, 1991.

[6] Moran, J. *An Introduction to Theoretical and Computational Aerodynamics*, John Wiley & Sons, New York, 1984. pp. 103-112, 118-123, 260-287.

[7] Karamcheti, K., *Principles of Ideal-Fluid Aerodynamics*, John Wiley & Sons, New York, 1966.

[8] Ashley, H, and Landahl, M., *Aerodynamics of Wings and Bodies*, Addison-Wesley, Reading, 1965 (republished in paperback by Dover Publishing).

[9] Curle, N., and Davis, H.J., *Modern Fluid Dynamics*, Volume 1: Incompressible Flow, Van Nostrand, London, 1968.

[10] Houghton, E.L., and Carpenter, P.W., *Aerodynamics for Engineering Students*, 4th Ed., Halsted Press, New York, 1993, pp. 257-265, 203-211.

[11] Kuethe, A.M., and Chow, C-Y., *Foundations of Aerodynamics*, 4th Ed., John Wiley, New York, 1986, pp. 128-137.

[12] Abbott, I.H., and von Doenhoff, A.E., *Theory of Wing Sections*, Dover, New York, 1959.

[13] Jones, R.T., *Wing Theory*, Princeton University Press, Princeton, 1990.

[14] Warner, E.P., *Airplane Design: Performance*, McGraw-Hill, New York, 1936.

[15] McGhee, Robert J., and Beasley, William D., "Low Speed Aerodynamic Characteristics of a 17-Percent-Thick Airfoil Section Designed for General Aviation Applications," NASA TN D-7428, 1973.

[16] Kroo, Ilan, "Aerodynamic Analyses for Design and Education," AIAA Paper 92-2664, June 1992.

[17] Volpe, G., "Inverse Airfoil Design: A Classical Approach Updated for Transonic Applications," in *Applied Computational Aerodynamics*, ed. by P.A. Henne, AIAA Progress in Astronautics and Aeronautics, Vol. 125, AIAA, New York, 1990, pp. 191-220.

[18] Labrujere, Th. E., and Sloof, J.W., "Computational Methods for the Aerodynamic Design of Aircraft Components, Ann. Rev. of Fluid Mech., 1993, Vol. 25, pp.183-214.

[19] Bristow, D.R., "A New Surface Singularity Method for Multi-Element Airfoil Analysis and Design," AIAA Paper 76-20, Jan. 1976.

[20] Aidala, P.V., Davis, W.H., Jr., and Mason, W.H., "Smart Aerodynamic Optimization," AIAA Paper 83-1863, July 1983.

[21] Hess, J. L. "The Problem of Three-Dimensional Lifting Potential Flow and Its Solution by Means of Surface Singularity Distributions", *Computer Methods in Applied Mechanics and Engineering* 4 (1974) pp. 283-319.

[22] Carmichael, R.L., and Erickson, L.L., "PAN AIR - A Higher Order Panel Method for Predicting Subsonic or Supersonic Linear Potential Flows About Arbitrary Configurations," AIAA Paper No. 81-1255, June 1981.

[23] PAN AIR User's Class Short Course Presentation Material, 1981.

[24] Tinoco, E.N., Ball, D.N., and Rice, F.A. II, "PAN AIR Analysis of a Transport High-Lift Configuration, *Journal of Aircraft*, Vol. 24, No. 3, March 1987, pp. 181-188.

[25] Magnus, A.E., and Epton, M.A., "PAN AIR - A Computer Program for Predicting Subsonic or Supersonic Linear Potential Flows About Arbitrary Configurations Using a Higher Order Panel Method," Volume I - Theory Document (Version 1.0), NASA CR 3251, April 1980.

[26] Margason, R.J., Kjelgaard, S.O., Sellers, W.L., Moriis, C.E.K., Jr., Walkley, K.B., and Shields, E.W., "Subsonic Panel Methods - A Comparison of Several Production Codes," AIAA Paper 85-0280, Jan. 1985.

[27] Ashby, D.L., Dudley, M.R., Iguchi, S.K., Browne, L., and Katz, J., "Potential Flow Theory and Operation Guide for the Panel Code PMARC," NASA TM 102851, Jan. 1991.